Dynamic Formation of Self-Organized Corner-Connected Square Metallocycles by Stoichiometric Control

Víctor Blanco, Marcos D. Garcia, Carlos Platas-Iglesias, Carlos Peinador*, and José M. Quintela*.

Departamento de Química Fundamental, Facultad de Ciencias, Universidade da Coruña. Campus A Zapateira, 15071, A Coruña, Spain

E-mail: carlos.peinador@udc.es (C.P.); jqqoqf@udc.es (J.M.Q.)

Supporting Information

Table of Contents

General Methods 3

Metallocycle 5a·2BF_4·12NO_3 3

Metallocycle 6a·4BF_4·16NO_3 3

Metallocycle 7a·6BF_4·20NO_3 3

Metallocycle 5a·2BF_4·4OTf·8PF_6 4

Metallocycle 6a·4BF_4·4OTf·12PF_6 4

Metallocycle 7a·6BF_4·4OTf·16PF_6 4

Metallocycle 5b·14PF_6 4

Metallocycle 6b·20PF_6 4

Figure S1: ^{1}H NMR (D_2O, 500 MHz) spectrum of 5a·2BF_4·12NO_3 6

Figure S2: ^{13}C NMR (D_2O, 125 MHz) spectrum of 5a·2BF_4·12NO_3 6

Figure S3: HSQC (D_2O, 500 MHz and 125 MHz) spectrum of 5a·2BF_4·12NO_3 7

Figure S4: HMBC (D_2O, 500 MHz and 125 MHz) spectrum of 5a·2BF_4·12NO_3 7

Figure S5: COSY (D_2O, 500 MHz) spectrum of 5a·2BF_4·12NO_3 8

Figure S6: ^{1}H NMR (D_2O, 500 MHz) spectrum of 6a·4BF_4·16NO_3 9

Figure S7: ^{13}C NMR (D_2O, 125 MHz) spectrum of 6a·4BF_4·16NO_3 9

Figure S8: ^{1}H NMR (D_2O, 500 MHz) spectrum of 7a·6BF_4·20NO_3 10

Figure S9: ^{13}C NMR (D_2O, 125 MHz) spectrum of 7a·6BF_4·20NO_3 10

Figure S10: Partial ^{1}H NMR spectra (D_2O, 298 K, 500 MHz) of a) 4a·8NO_3, b) 5a·2BF_4·12NO_3, c) 6a·4BF_4·16NO_3, d) 7a·6BF_4·20NO_3. 11

Figure S11: ^{1}H NMR (CD_3CN, 500 MHz) spectrum of 5a·2BF_4·4OTf·8PF_6 12

Figure S12: ^{13}C NMR (CD_3CN, 125 MHz) spectrum of 5a·2BF_4·4OTf·8PF_6 12

Figure S13: HSQC (CD_3CN, 500 and 125 MHz) spectrum of 5a·2BF_4·4OTf·8PF_6 13

Figure S14: HMBC (CD_3CN, 500 and 125 MHz) spectrum of $5a{\cdot}2BF_4{\cdot}4OTf{\cdot}8PF_6$ 13

Figure S15: COSY (CD_3CN, 500 MHz) spectrum of $5a{\cdot}2BF_4{\cdot}4OTf{\cdot}8PF_6$ 14

Figure S16: DOSY (CD_3CN, 500 MHz) spectrum of $5a{\cdot}2BF_4{\cdot}4OTf{\cdot}8PF_6$ 15

Figure S17: Fitting of I/I_o for some ^1H signals of compound $5a{\cdot}2BF_4{\cdot}4OTf{\cdot}8PF_6$ to a simple one-component exponential. 15

Figure S18: ^1H NMR (CD_3CN, 500 MHz) spectrum of $6a{\cdot}4BF_4{\cdot}4OTf{\cdot}12PF_6$ 16

Figure S19: ^{13}C NMR (CD_3CN, 125 MHz) spectrum of $6a{\cdot}4BF_4{\cdot}4OTf{\cdot}12PF_6$ 16

Figure S20: DOSY (CD_3CN, 500 MHz) spectrum of $6a{\cdot}4BF_4{\cdot}4OTf{\cdot}12PF_6$ 17

Figure S21: Fitting of I/I_o for some ^1H signals of compound $6a{\cdot}4BF_4{\cdot}4OTf{\cdot}12PF_6$ to a simple one-component exponential. 17

Figure S22: ^1H NMR (CD_3CN, 500 MHz) spectrum of $7a{\cdot}6BF_4{\cdot}4OTf{\cdot}16PF_6$ 18

Figure S23: ^{13}C NMR (CD_3CN, 125 MHz) spectrum of $7a{\cdot}6BF_4{\cdot}4OTf{\cdot}16PF_6$ 18

Figure S24: DOSY (CD_3CN, 500 MHz) spectrum of $7a{\cdot}6BF_4{\cdot}4OTf{\cdot}16PF_6$ 19

Figure S25: Fitting of I/I_o for some ^1H signals of compound $7a{\cdot}6BF_4{\cdot}4OTf{\cdot}16PF_6$ to a simple one-component exponential. 19

Figure S26: Partial ^1H NMR (CD_3CN, 500 MHz) spectra of: a) $4a{\cdot}4OTf{\cdot}4PF_6$, b) $5a{\cdot}2BF_4{\cdot}4OTf{\cdot}8PF_6$, c) $6a{\cdot}4BF_4{\cdot}4OTf{\cdot}12PF_6$, d) $7a{\cdot}6BF_4{\cdot}4OTf{\cdot}16PF_6$ 20

Figure S27: ^1H NMR (CD_3CN, 500 MHz) spectrum of $5b{\cdot}14PF_6$ 21

Figure S28: ^{13}C NMR (CD_3CN, 125 MHz) spectrum of $5b{\cdot}14PF_6$ 21

Figure S29: ESI-MS of $5b{\cdot}14PF_6$. 22

Figure S30: Observed (top) and theoretical (bottom) isotopic distribution for the fragment $[5b{\cdot}6PF_6]^{+8}$. 22

Figura S31: ^1H NMR (CD_3CN, 500 MHz) spectrum of $6b{\cdot}20PF_6$ 23

Figure S32: ^{13}C NMR (CD_3CN, 125 MHz) spectrum of $6b{\cdot}20PF_6$ 23

Figure 33: ESI-MS of $6b{\cdot}20PF_6$ 24

Figure 34: Observed (top) and theoretical (bottom) isotopic distribution for the fragment $[6b{\cdot}14PF_6]^{+6}$. 24

Dynamic formation of dimer, trimer, and tetramer in D_2O. 25

Determination of diffusion coefficients from theoretical models 26

Table S1. Diffusion coefficients and dimensions of metallocycles 27

Computational Methods 28

Figure 35: Calculated structures of 4a-7a. 28

General Methods

Ligand **1**[1], (en)Pd(OTf)$_2$, and (en)Pt(OTf)$_2$[2] were prepared according to published procedures. All other reagents used were commercial grade chemicals from freshly opened containers. Milli-Q water was purified with a Millipore Gradient A10 apparatus. Merck 60 F_{254} foils were used for thin layer chromatography, and Merck 60 (230-400 mesh) silica gel was used for flash chromatography. Proton and carbon nuclear magnetic resonance spectra were recorded on a Bruker Avance 300 or Bruker Avance 500 equipped with a dual cryoprobe for ^{1}H and ^{13}C, using the deuterated solvent as lock and the residual protiated solvent as internal standard. DOSY experiments were referenced using the value 1.92×10^{-9} m^2s^{-1} for the DHO signal in D_2O at 298 K[3] and the value 2.18×10^{-9} m^2s^{-1} for the CHD_2CN signal in CD_3CN at 298 K.[4] Mass spectrometry experiments were carried out in a LC-Q-q-TOF Applied Biosystems QSTAR Elite spectrometer for low- and high-resolution ESI.

Metallocycle **5a**·2BF_4·12NO_3

To a solution of Pd$(CH_3CN)_4(BF_4)_2$ (2.2 mg, 5.0×10^{-3} mmol) in D_2O (2.0 mL), ligand **1**·2NO_3 (9.0 mg, 0.020 mmol) and (en)Pd$(NO_3)_2$ (2.9 mg, 0.010 mmol) were added. *^{1}H NMR (500 MHz, D_2O) δ*: 2.93 (8H, s); 7.48 (8H, m); 8.00 (8H, d, *J* = 6.9 Hz); 8.04 (8H, d, *J* = 6.9 Hz); 8.52 (16H, m); 8.95 (8H, d, *J* = 6.9 Hz); 9.14 (8H, d, *J* = 5.5 Hz); 9.40 (16H, m); *^{13}C NMR (125 MHz, D_2O) δ*: 48.8 (CH_2); 77.7 (CH_2); 125.2 (CH); 125.8 (CH); 127.4 (CH); 127.5 (CH); 144.2 (C); 144.9 (C); 145.8 (CH); 152.1 (CH); 152.3 (CH); 154.6 (C); 154.9 (C).

Metallocycle **6a**·4BF_4·16NO_3

To a solution of Pd$(CH_3CN)_4(BF_4)_2$ (3.0 mg, 6.7×10^{-3} mmol) in D_2O (2.0 mL), ligand (9.0 mg, 0.020 mmol) and (en)Pd$(NO_3)_2$ (1.5 mg, 5.0×10^{-3} mmol) were added.

1·2NO_3 *NMR (500 MHz, D_2O) δ*: 2.92 (8H, s); 7.48 (12H, m); 8.00 (8H, d, *J* = 7.0 Hz); 8.04 (16H, d, *J* = 4.9 Hz); 8.52 (24H, m); 8.95 (8H, d, *J* = 6.8 Hz); 9.14 (16H, d, *J* = 6.4 Hz); 9.40 (24H, m); *^{13}C NMR (125 MHz, D_2O) δ*: 46.8 (CH_2); 77.7 (CH_2); 125.3 (CH); 125.8 (CH); 127.4 (CH); 127.5 (CH); 144.2 (C); 144.9 (C); 145.8 (CH); 152.1 (CH); 152.3 (CH); 154.6 (C); 154.9 (C).

Metallocycle **7a**·6BF_4·20NO_3

To a solution of Pd$(CH_3CN)_4(BF_4)_2$ (3.3 mg, 7.5×10^{-3} mmol) in D_2O (2.0 mL), ligand **1**·**2**NO_3 (9.0 mg, 0.020 mmol) and (en)Pd$(NO_3)_2$ (1.5 mg, 5.0×10^{-3} mmol) were added. *^{1}H NMR (500 MHz, D_2O) δ*: 2.93 (8H, s); 7.48 (16H, m); 8.00 (8H, d, *J* = 6.9 Hz); 8.04 (24H, d, *J* = 5.2 Hz); 8.52 (32H, m); 8.96 (8H, d, *J* = 6.8 Hz); 9.14 (24H, d, *J* = 6.1 Hz); 9.40 (32H, m); *^{13}C NMR (125 MHz, D_2O) δ*: 46.8 (CH_2); 77.7 (CH_2); 125.3 (CH); 125.8 (CH); 127.4 (CH); 127.5 (CH); 144.2 (C); 144.9 (C); 145.8 (CH); 152.1 (CH); 152.3 (CH); 154.6 (C); 154.9 (C).

---

[1] (a) V. Blanco, M. Chas, D. Abella, C. Peinador and J. M. Quintela, *J. Am. Chem. Soc.* 2007, **129**, 13978; (b) V. Blanco, M. Chas, D. Abella, E. Pía, C. Platas-Iglesias, C. Peinador and J. M. Quintela, *Org. Lett*. 2008, **10**, 409.

[2] (a) C. Diver and G. A. Lawrance, *J. Chem. Soc., Dalton Trans.* 1988, 931. (b) P. de Wolf, S. L. Heath and J. M. Thomas, *Inorg. Chim. Acta* 2003, 280.

[3] L. G. Longsworth, *Phys. Chem*. 1960, 1914.

[4] R. -S. Luo, X. -A. Mao, Z. -Q. Pan and Q.-H. Luo, *Spectrochim. Acta A: Mol. Biomol. Spectrosc.* 2000, **55**, 1675.

Metallocycle 5a·2BF_4·4OTf·8PF_6

To a solution of $Pd(CH_3CN)_4(BF_4)_2$ (2.2 mg, 5.0×10^{-3} mmol) in CD_3CN (2.0 mL), ligand **1**·2PF_6 (12.5 mg, 0.020 mmol) and (en)$Pd(OTf)_2$ (5.6 mg, 0.010 mmol) were added. *^{1}H NMR (500 MHz, CD_3CN) δ*: 2.90 (8H, s); 4.39 (8H, s); 7.13 (8H, s); 7.97 (16H, m); 8.42 (16H, m); 8.99 (8H, m); 9.13 (16H, m); 9.20 (8H, m); *^{13}C NMR (125 MHz, CD_3CN) δ*: 47.9 (CH_2); 78.3 (CH_2); 126.2 (CH); 127.0 (CH); 128.5 (CH); 128.7 (CH); 145.0 (C); 145.7 (C); 147.1 (CH); 147.1 (CH); 147.1 (CH); 153.5 (CH); 154.0 (CH); 155.6 (C); 155.8 (C).

Metallocycle 6a·4BF_4·4OTf·12PF_6

To a solution of $Pd(CH_3CN)_4(BF_4)_2$ (3.0 mg, 6.7×10^{-3} mmol) in CD_3CN (2.0 mL), ligand **1**·2PF_6 (12.5 mg, 0.020 mmol) and (en)$Pd(OTf)_2$ (3.7 mg, 6.7×10^{-3} mmol) were added. *^{1}H NMR (500 MHz, CD_3CN) δ*: 2.90 (8H, s); 4.36 (8H, s); 7.12 (12H, s); 7.98 (24H, m); 8.41 (24H, m); 8.98 (8H, m); 9.12 (24H, m); 9.18 (16H, m); *^{13}C NMR (125 MHz, CD_3CN) δ*: 47.9 (CH_2); 78.4 (CH_2); 126.2 (CH); 127.0 (CH); 128.5 (CH); 128.7 (CH); 145.0 (C); 145.7 (C); 147.0 (CH); 147.0 (CH); 147.0 (CH); 153.5 (CH); 154.0 (CH); 155.6 (C); 155.8 (C).

Metallocycle 7a·6BF_4·4OTf·16PF_6

To a solution of $Pd(CH_3CN)_4(BF_4)_2$ (3.3 mg, 7.5×10^{-3} mmol) in CD_3CN (2.0 mL), ligand **1**·2PF_6 (12.5 mg, 0.020 mmol) and (en)$Pd(OTf)_2$ (2.8 mg, 5.0×10^{-3} mmol) were added.*^{1}H NMR (500 MHz, CD_3CN) δ*: 2.90 (8H, s); 4.35 (8H, s); 7.12 (16H, s); 7.97 (32H, m); 8.41 (32H, m); 8.98 (8H, m); 9.11 (32H, m); 9.18 (24H, m); *^{13}C NMR (125 MHz, CD_3CN) δ*: 47.9 (CH_2); 78.4 (CH_2); 126.2 (CH); 127.0 (CH); 128.5 (CH); 128.7 (CH); 145.1 (C); 145.8 (C); 147.0 (CH); 147.1 (CH); 153.5 (CH); 154.0 (CH); 155.6 (C); 155.8 (C).

Metallocycle 5b·14PF_6

A solution of $Pt(CH_3CN)_2Cl_2$ (2.9 mg, 8.4×10^{-3} mmol), AgOTf (4.3 mg, 16.7×10^{-3} mmol), ligand **1**·2PF_6 (20.6 mg, 0.033 mmol) and (en)$Pt(OTf)_2$ (10.7 mg, 16.7×10^{-3} mmol) in CH_3CN (3.0 mL) was heated protected from light for 8d at 55ºC. The suspension was filtered over a cap of Celite® to remove AgCl and the solvent was removed under reduced pressure without heating. The crude product was suspended in water (17 mL) and ion exchange resin (Amberlite IRA-402, 0.50 g) was added. The mixture was stirred at room temperature for 24 h. The resin was removed by filtration and an excess of KPF_6 is added to the filtrate until no further precipitation was observed. The solid was filtered and washed with water to yield **5b**·14PF_6 as a grey solid (14.0 mg, 41 %). *^{1}H NMR (500 MHz, CD_3CN) δ*: 2.83 (8H, s); 5.05 (8H, s); 7.16 (8H, s); 7.96 (8H, m); 8.01 (8H, m); 8.45 (16H, m); 9.01 (8H, m); 9.15 (16H, m); 9.22 (8H, m); *^{13}C NMR (125 MHz, CD_3CN) δ*: 48.7 (CH_2); 78.4 (CH_2); 126.7 (CH); 127.4 (CH); 128.5 (CH); 128.7 (CH); 144.9 (C); 145.8 (C); 147.1 (CH); 147.2 (CH); 147.2 (CH); 154.3 (CH); 154.8 (CH); 155.3 (C); 155.5 (C). *HRMS-ESI* (*m/z*): calcd for $[M–5PF_6^-]^{5+}$ 662.8638, found 662.8639; calcd for $[M–6PF_6^-]^{6+}$ 528.2258, found 528.2255; calcd for $[M–8PF_6^-]^{8+}$ 359.9281, found 359.9284; calcd for $[M–9PF_6^-]^{9+}$ 303.8289, found 303.8289.

Metallocycle 6b·20PF_6

A solution of $Pt(CH_3CN)_2Cl_2$ (12.0 mg, 34.5×10^{-3} mmol), AgOTf (17.7 mg, 68.9×10^{-3} mmol), ligand **1**·2PF_6 (63.7 mg, 0.103 mmol) and (en)$Pt(OTf)_2$ (23.0 mg, 34.5×10^{-3} mmol) in CH_3CN (11.0 mL) was heated protected from light for 8d at 55ºC. The suspension was filtered over a cap of Celite® to remove AgCl and the solvent was removed under reduced pressure without heating. The crude product was suspended in water (25 mL) and ion exchange resin (Amberlite IRA-402, 1.00 g) was added. The mixture was stirred at room temperature for 24h. The resin was removed by filtration and an excess of KPF_6 is added to

the filtrate until no further precipitation was observed. The solid was filtered and washed with water to yield **6b**·20PF_6 as a brown solid (60.9 mg, 61%). *^{1}H NMR (500 MHz, CD_3CN) δ*: 2.83 (8H, s); 5.05 (8H, s); 7.16 (12H, s); 7.96 (24H, m); 8.42 (24H, m); 8.97 (8H, m); 9.07 (24H, m); 9.11 (16H, m); *^{13}C NMR (125 MHz, CD_3CN) δ*: 48.7 (CH_2); 78.4 (CH_2); 123.5 (CH); 126.7 (CH); 128.2(CH); 127.4 (CH); 128.5 (CH); 128.7 (CH); 144.9 (C); 145.8 (C); 146.8 (CH); 147.1 (CH); 147.2 (CH); 151.6 (CH); 154.2 (CH); 154.8 (CH); 155.5 (C). *HRMS-ESI* (*m/z*): calcd for [M–6PF_6^-]$^{6+}$ 814.4018, found 814.4044.

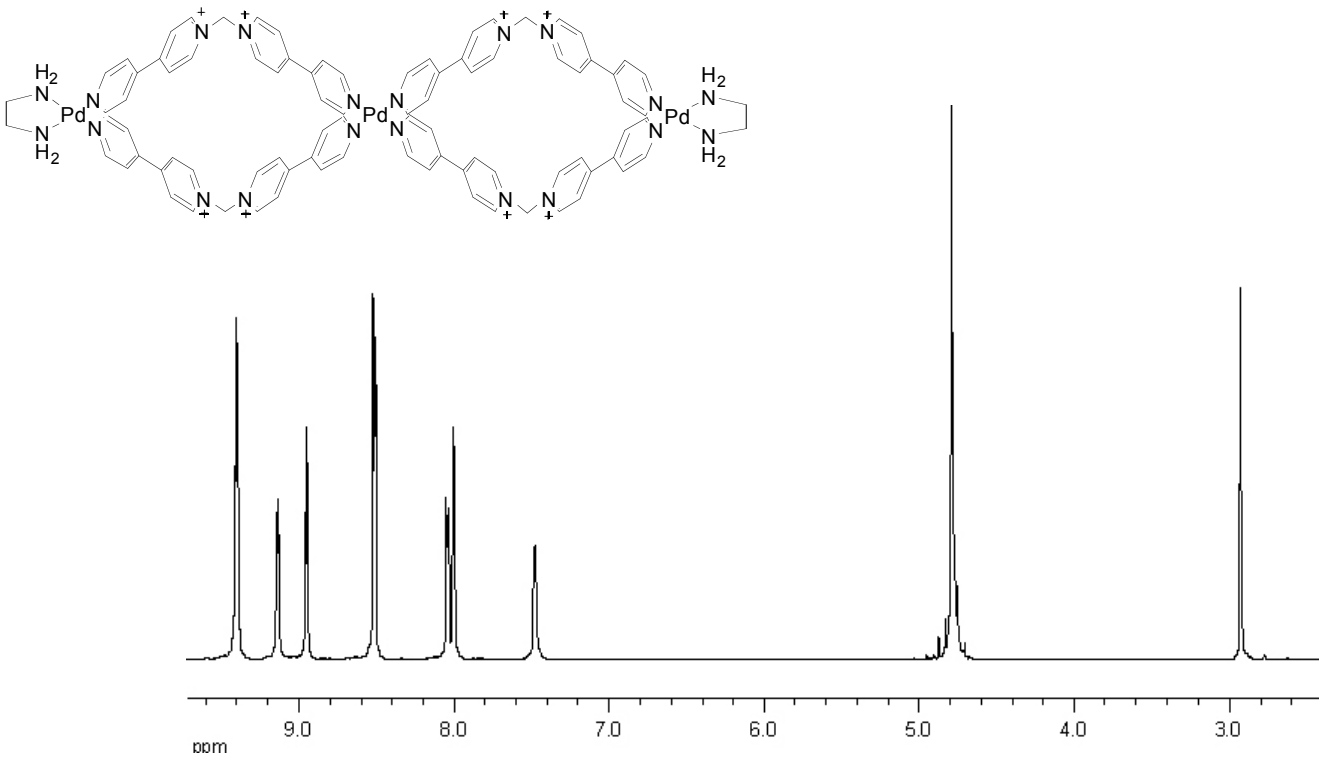

Figure S1: ^{1}H NMR (D_2O, 500 MHz) spectrum of **5a**·$2BF_4$·$12NO_3$

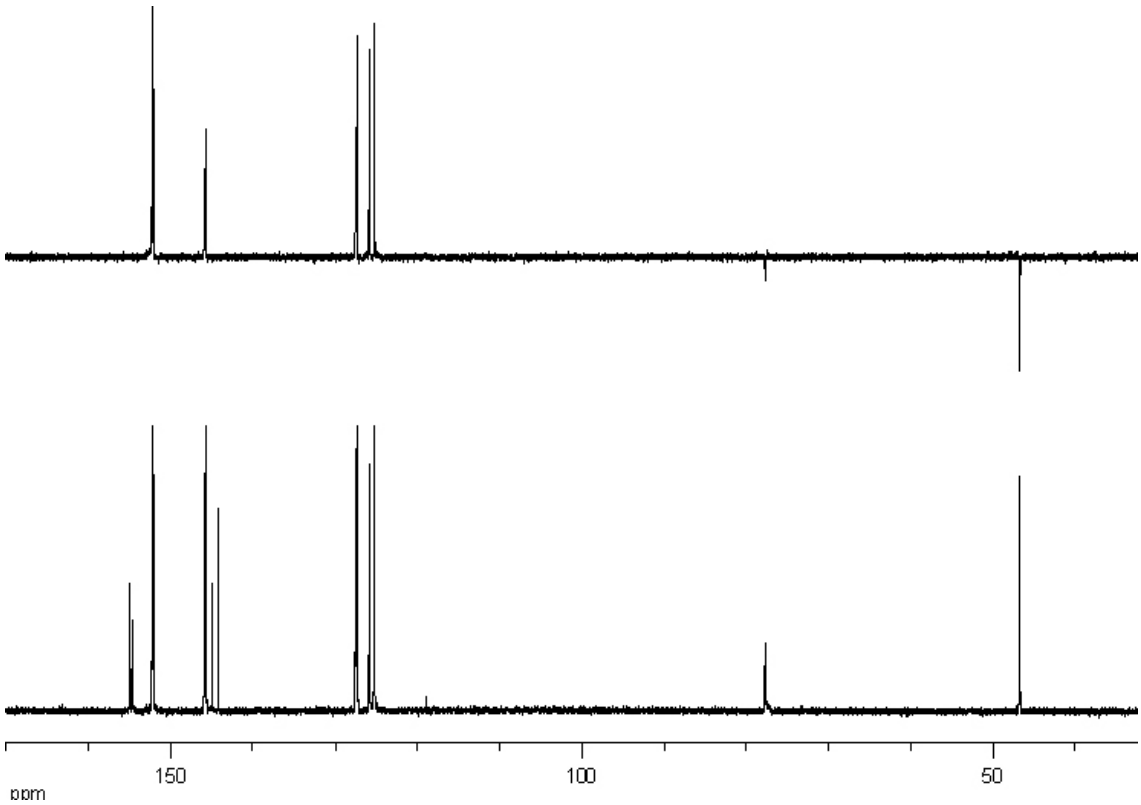

Figure S2: ^{13}C NMR (D_2O, 125 MHz) spectrum of **5a**·$2BF_4$·$12NO_3$

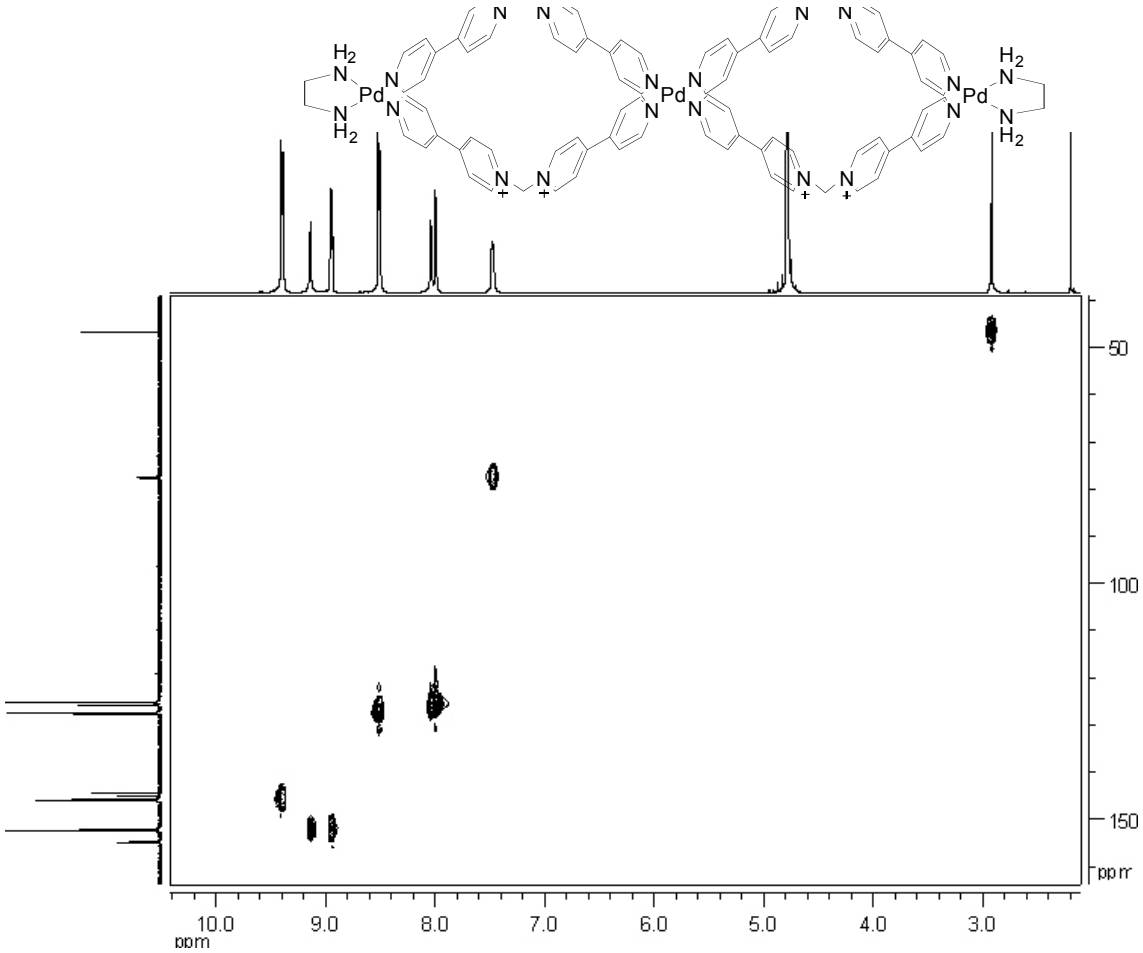

Figure S3: HSQC (D_2O, 500 MHz and 125 MHz) spectrum of **5a**·$2BF_4$·$12NO_3$

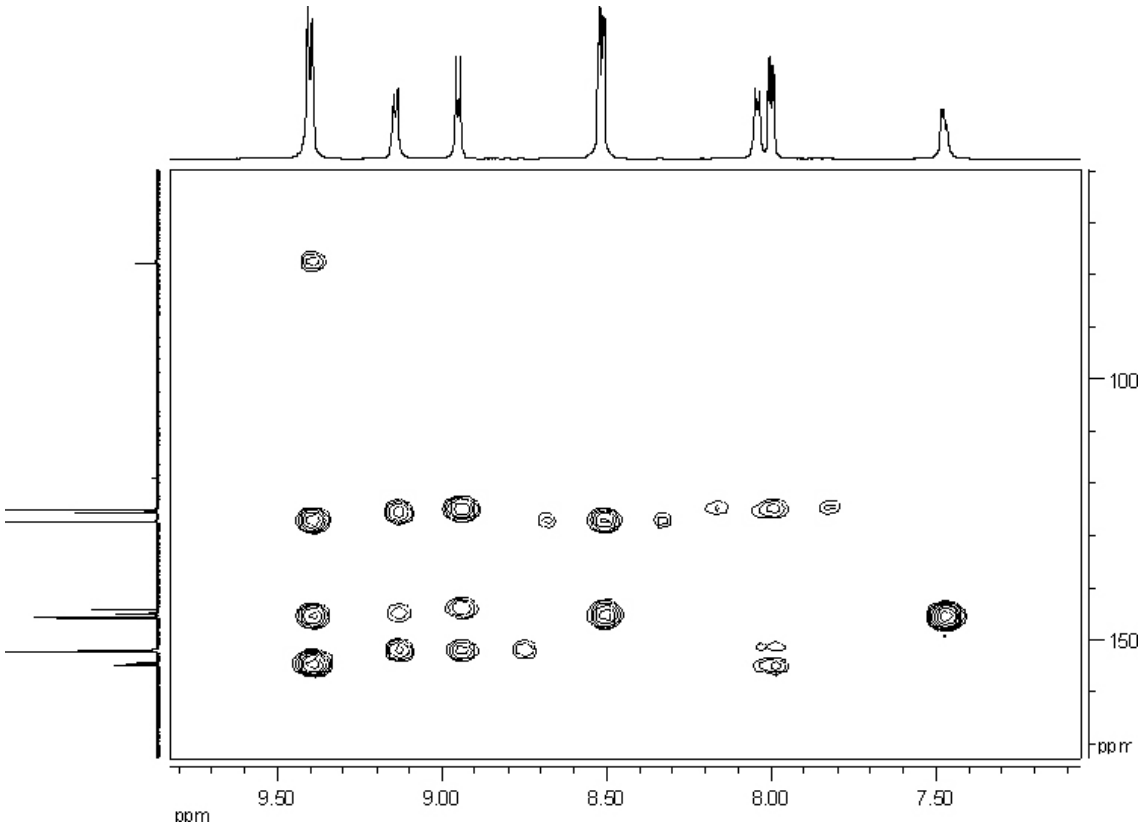

Figure S4: HMBC (D_2O, 500 MHz and 125 MHz) spectrum of **5a**·$2BF_4$·$12NO_3$

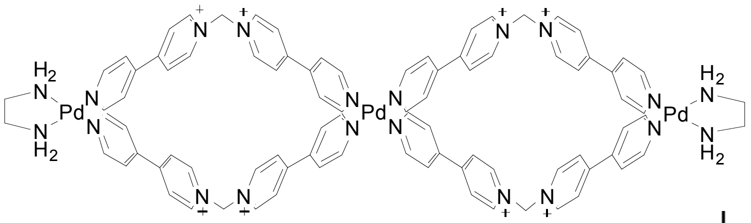

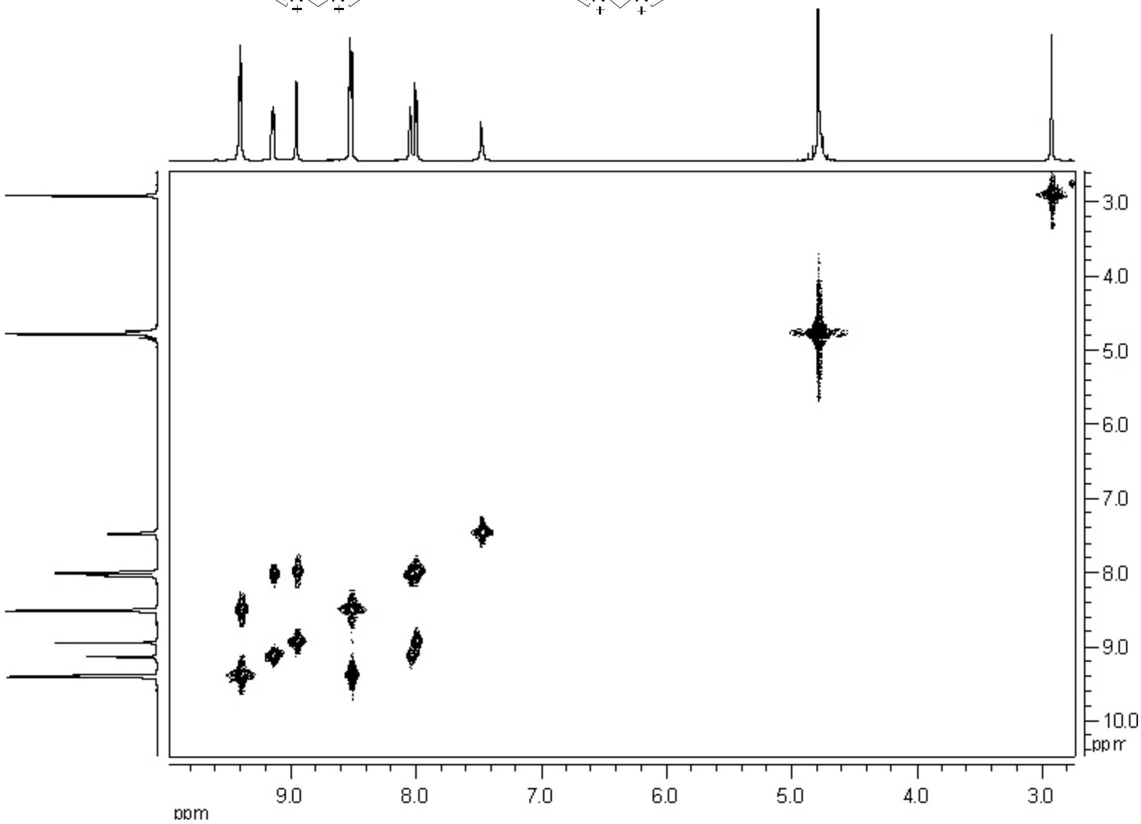

Figure S5: COSY (D_2O, 500 MHz) spectrum of **5a**·$2BF_4$·$12NO_3$

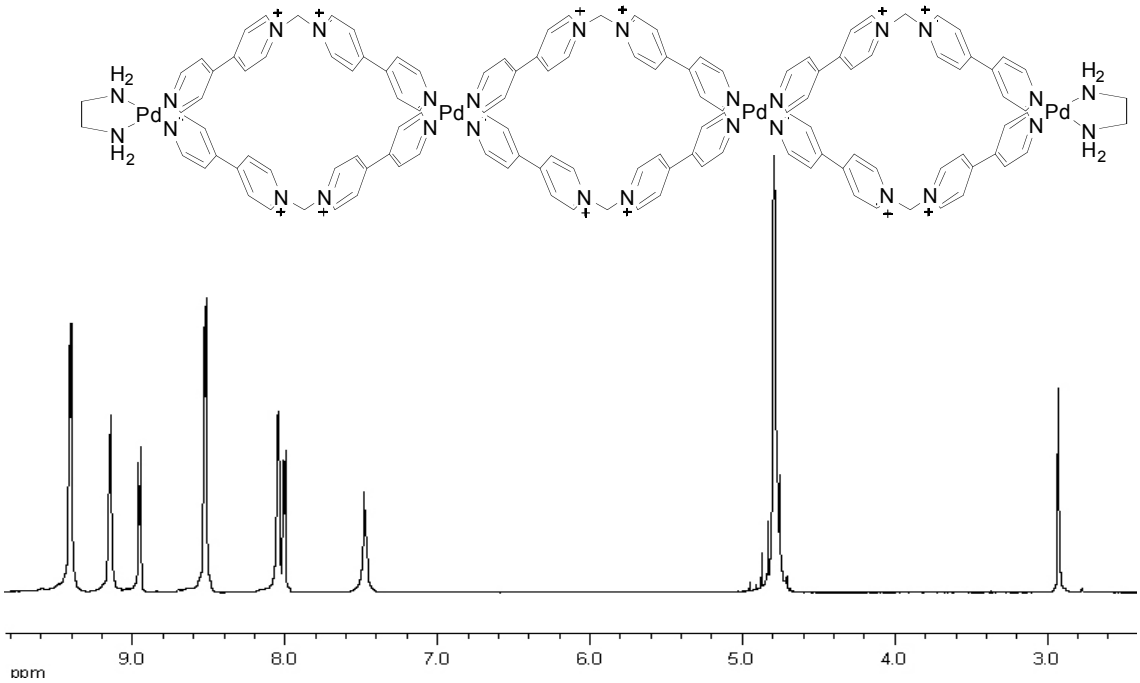

Figure S6: ^{1}H NMR (D_2O, 500 MHz) spectrum of **6a**·$4BF_4$·$16NO_3$

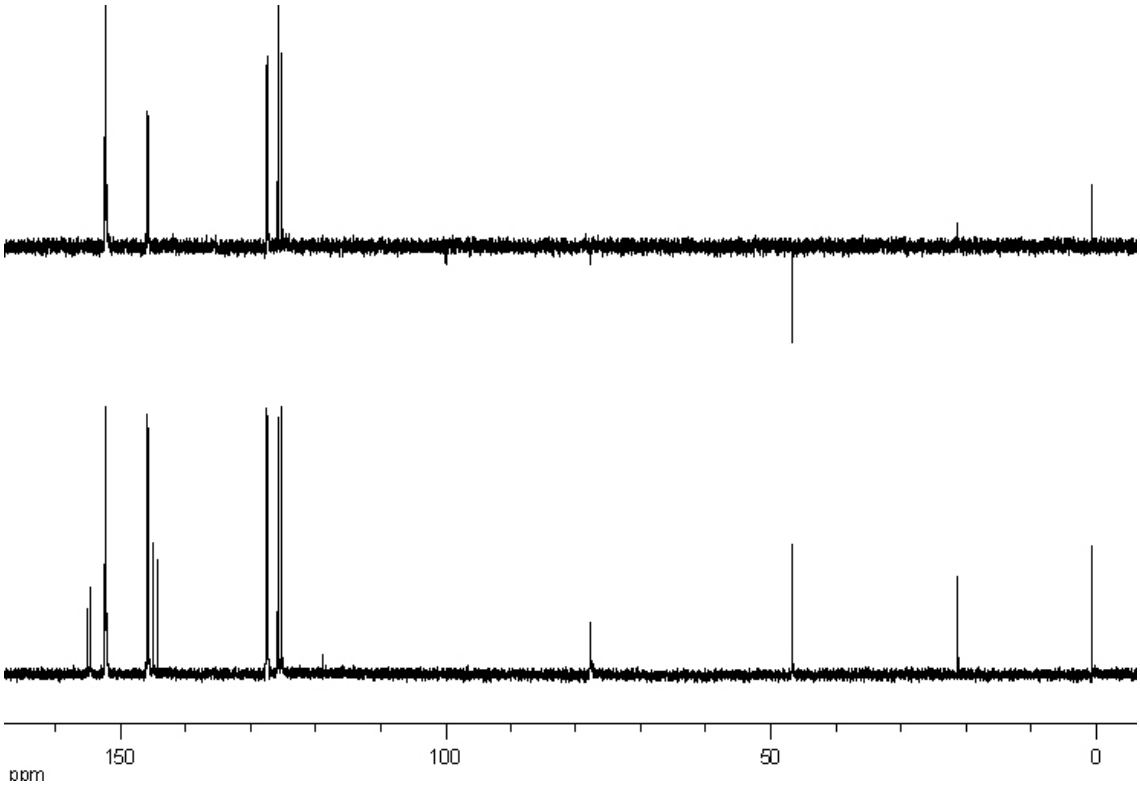

Figure S7: ^{13}C NMR (D_2O, 125 MHz) spectrum of **6a**·$4BF_4$·$16NO_3$

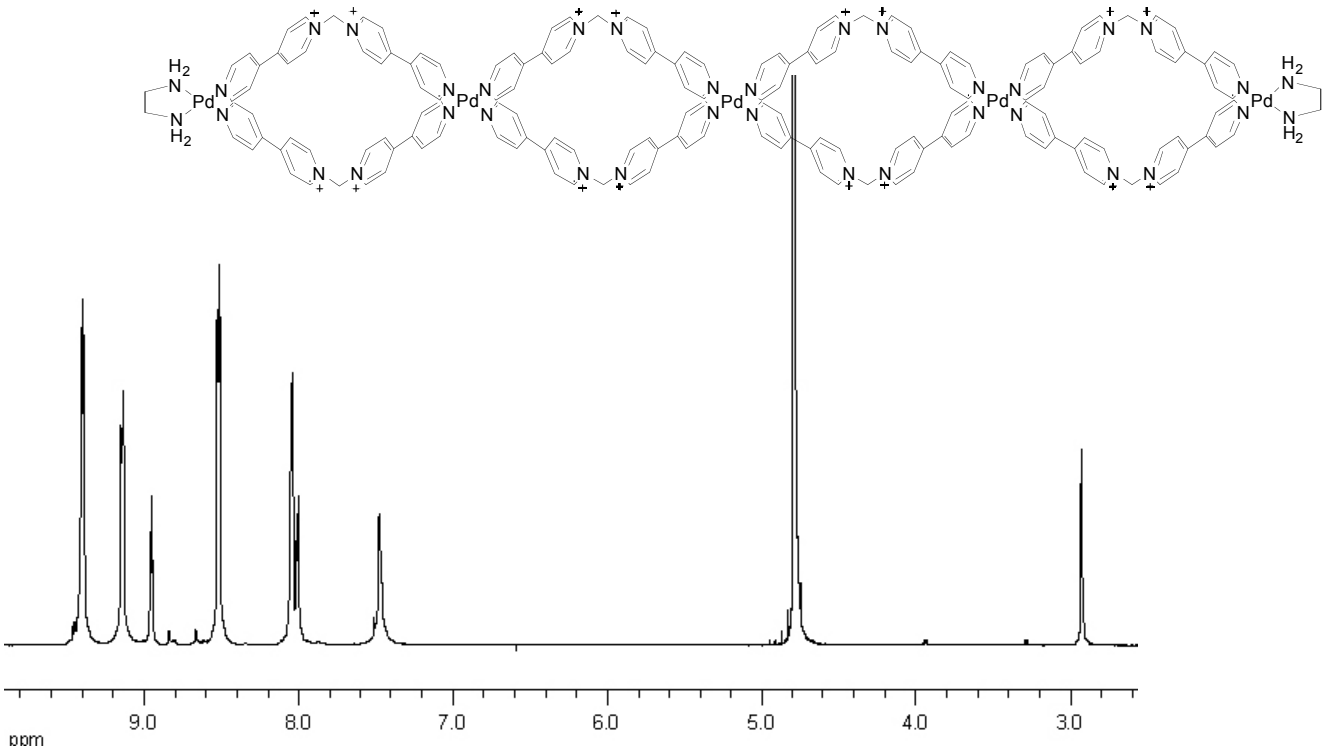

Figure S8: ^{1}H NMR (D_2O, 500 MHz) spectrum of **7a**·$6BF_4$·$20NO_3$

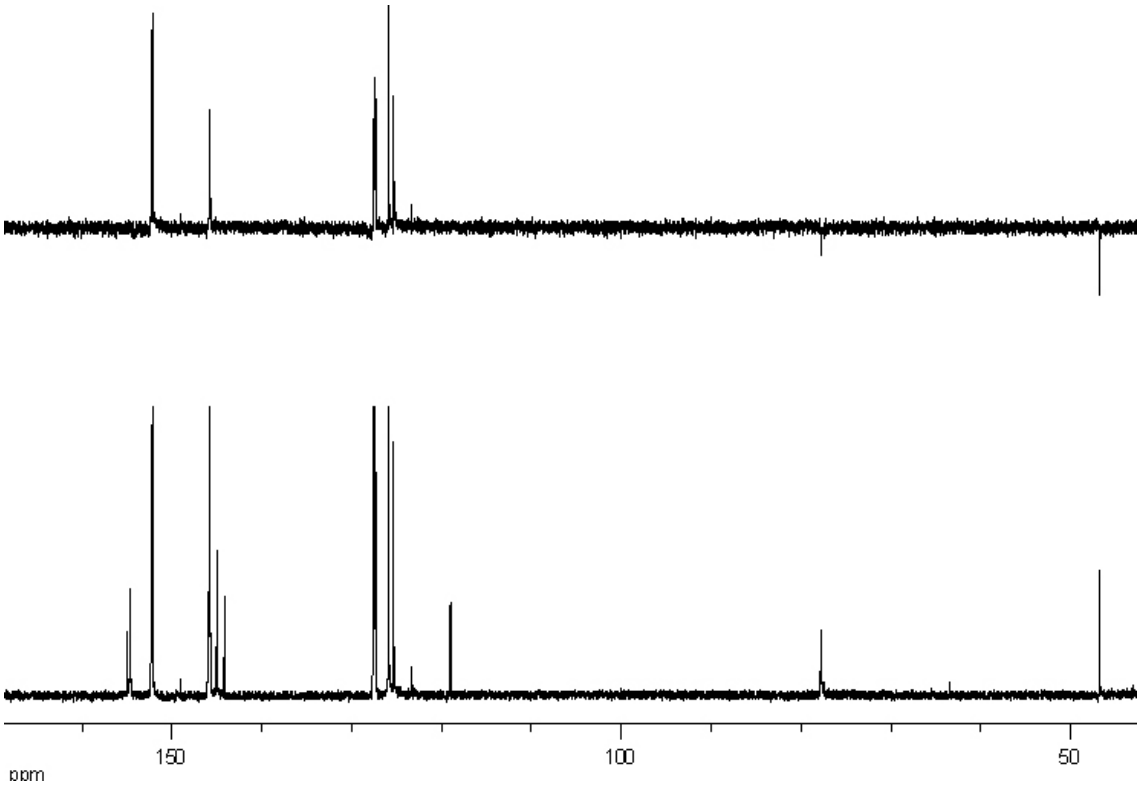

Figure S9: ^{13}C NMR (D_2O, 125 MHz) spectrum of **7a**·$6BF_4$·$20NO_3$

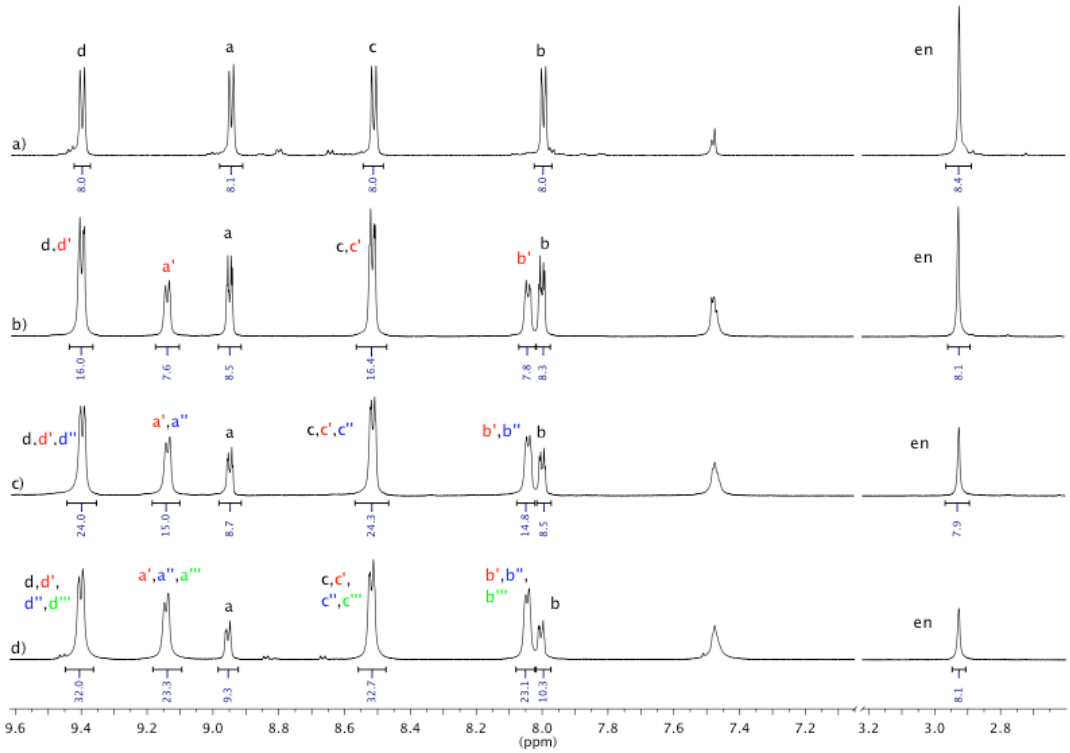

Figure S10: Partial ^{1}H NMR spectra (D_2O, 298 K, 500 MHz) of a) **4a**·8NO_3, b) **5a**·2BF_4·12NO_3, c) **6a**·4BF_4·16NO_3, d) **7a**·6BF_4·20NO_3.

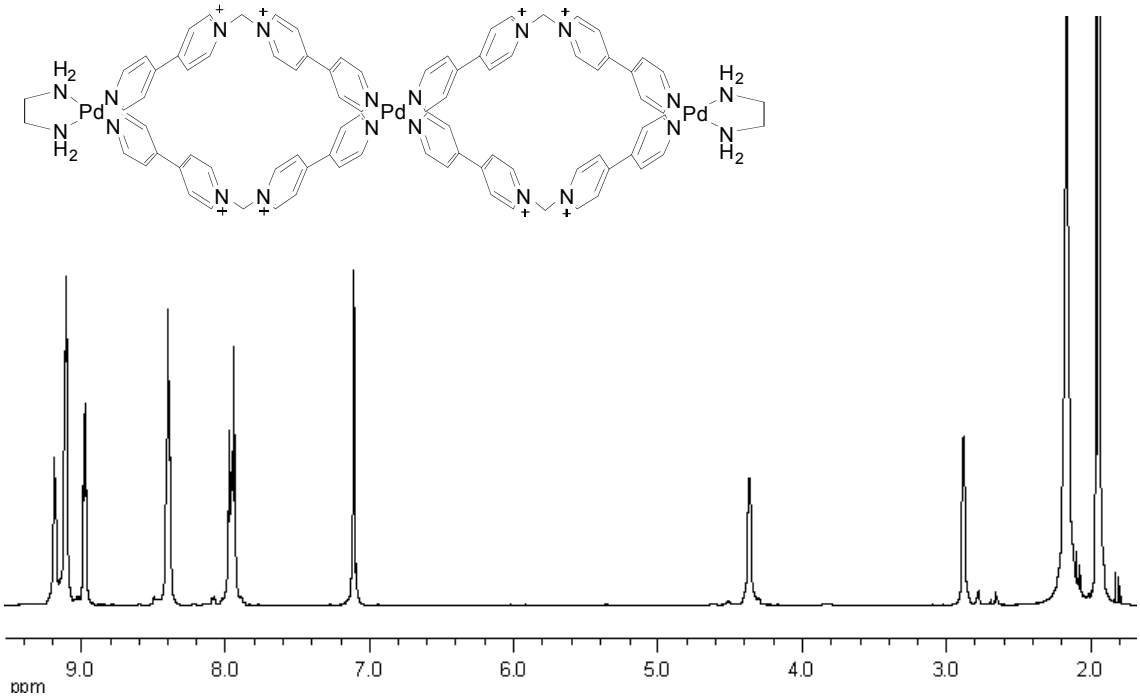

Figure S11: ^{1}H NMR (CD_3CN, 500 MHz) spectrum of **5a**·2BF_4·4OTf·8PF_6

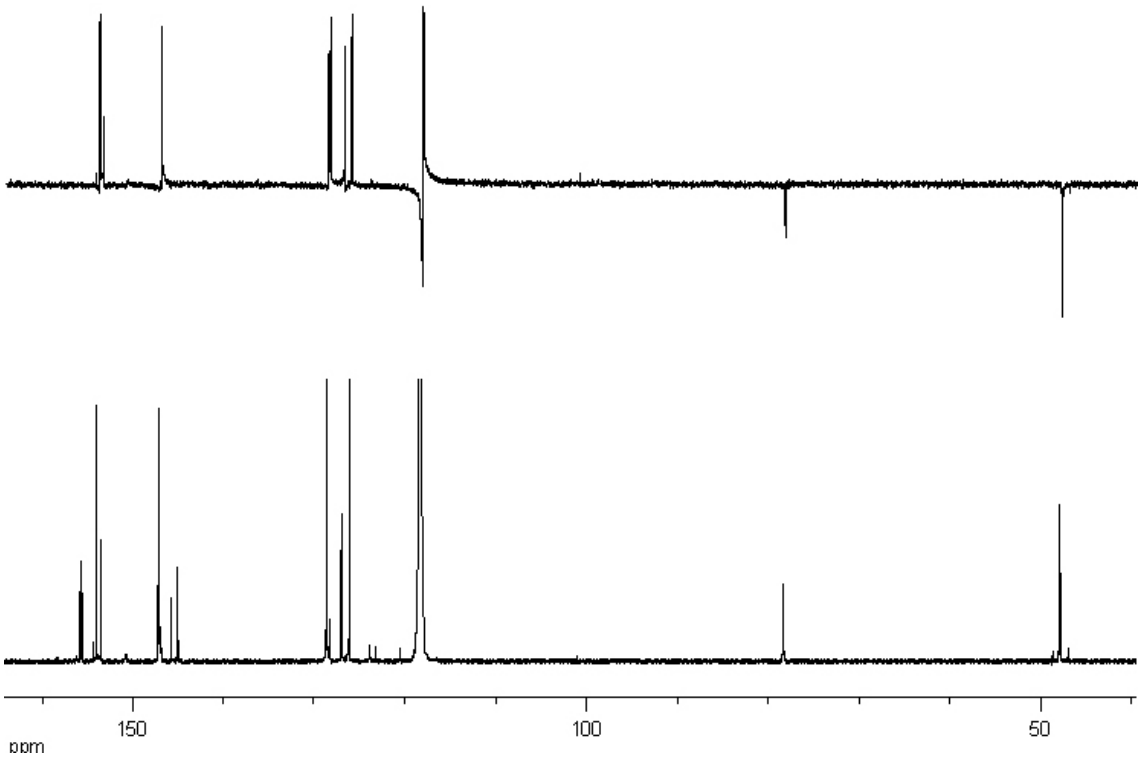

Figure S12: ^{13}C NMR (CD_3CN, 125 MHz) spectrum of **5a**·2BF_4·4OTf·8PF_6

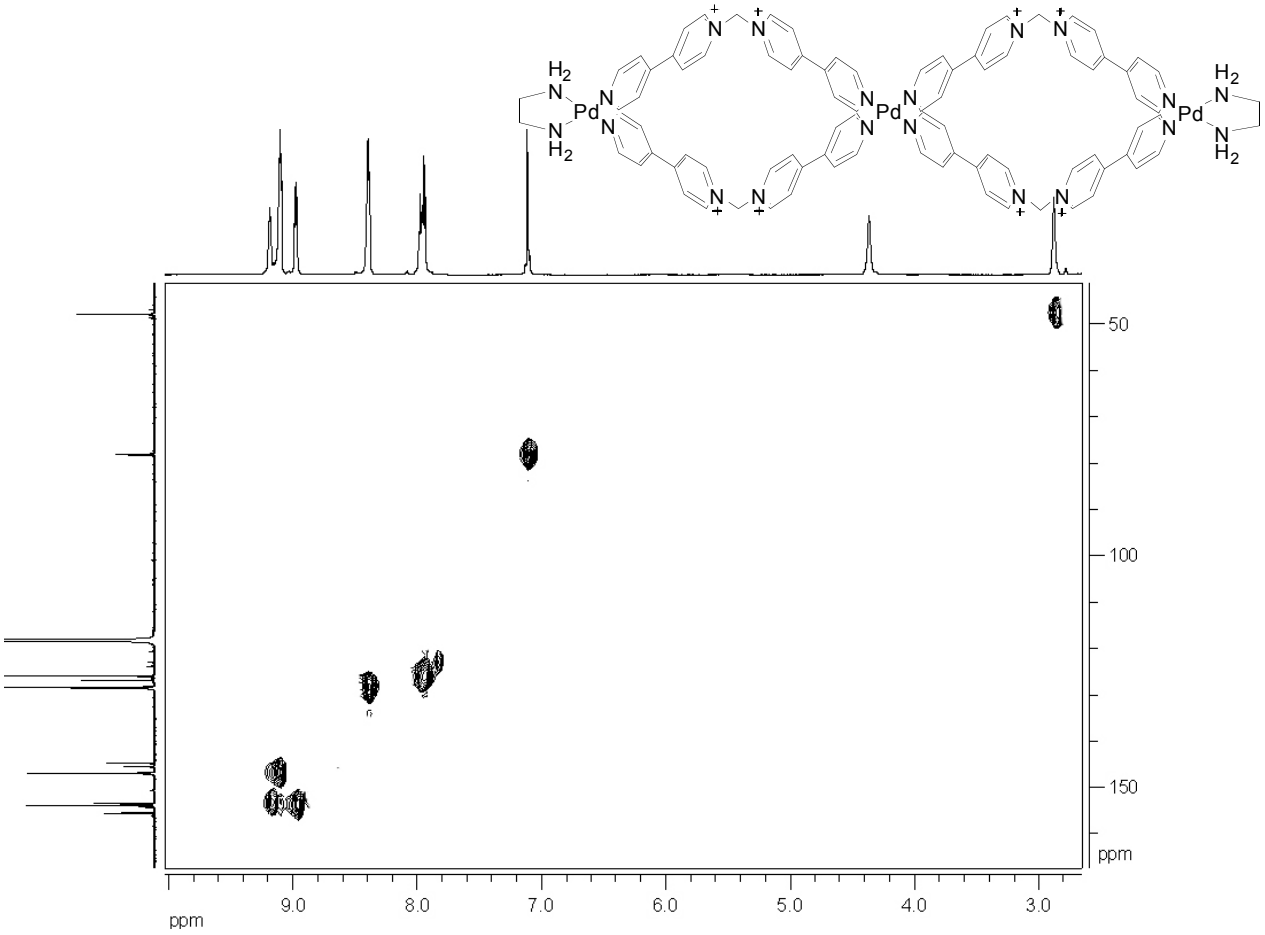

Figure S13: HSQC (CD_3CN, 500 and 125 MHz) spectrum of **5a**·$2BF_4$·4OTf·$8PF_6$

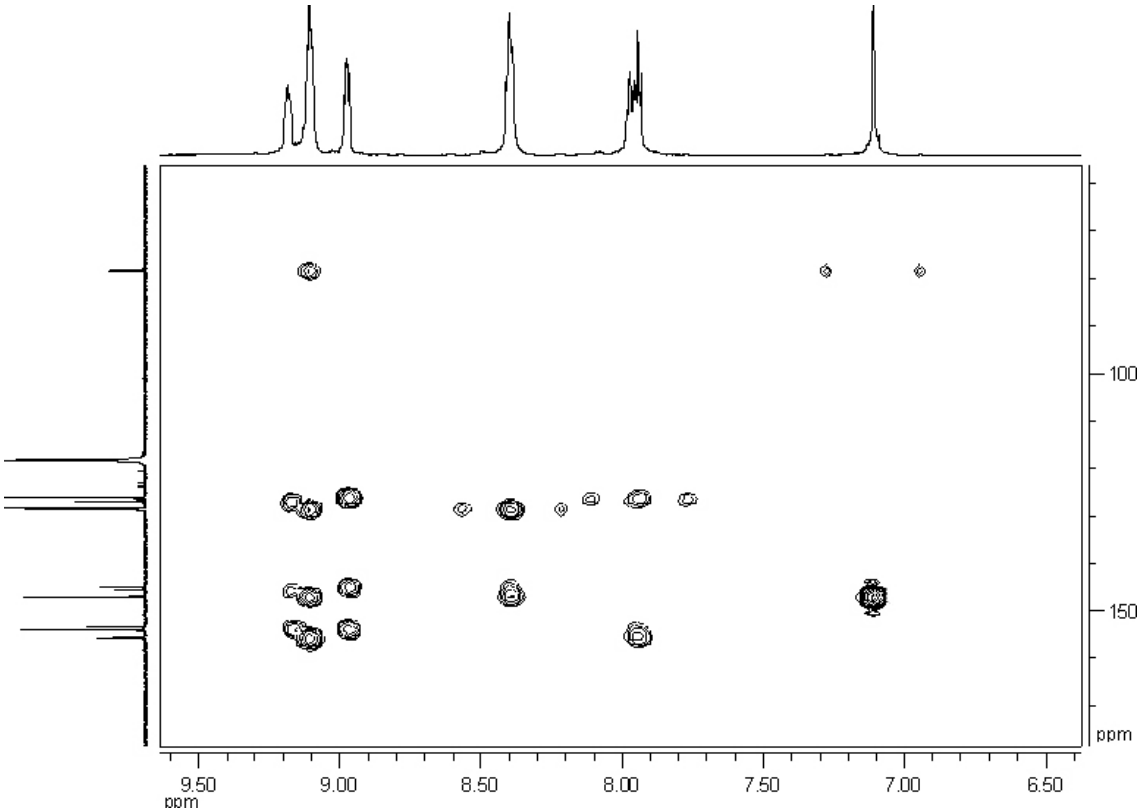

Figure S14: HMBC (CD_3CN, 500 and 125 MHz) spectrum of **5a**·$2BF_4$·4OTf·$8PF_6$

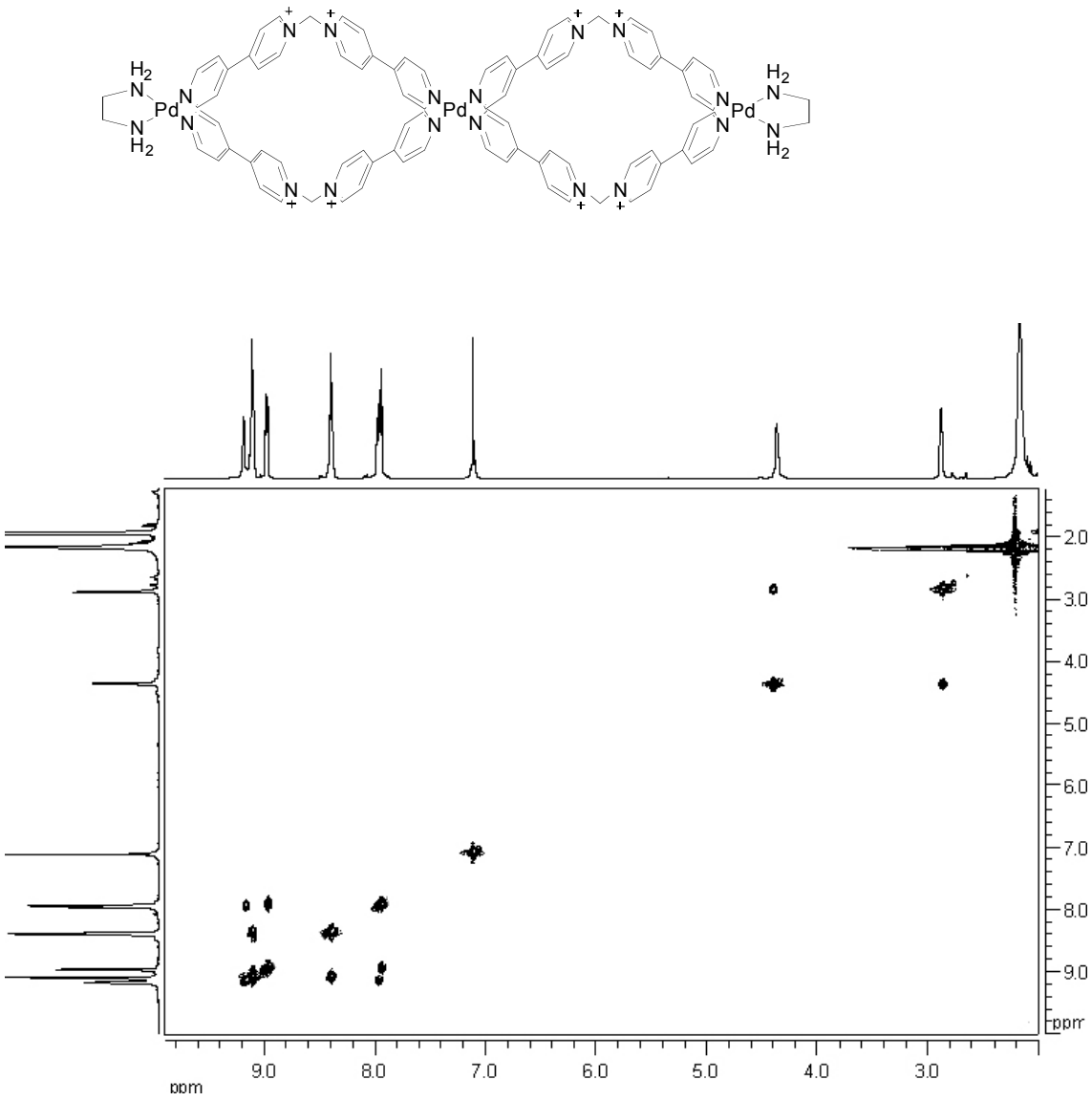

Figure S15: COSY (CD_3CN, 500 MHz) spectrum of **5a**·$2BF_4$·4OTf·$8PF_6$

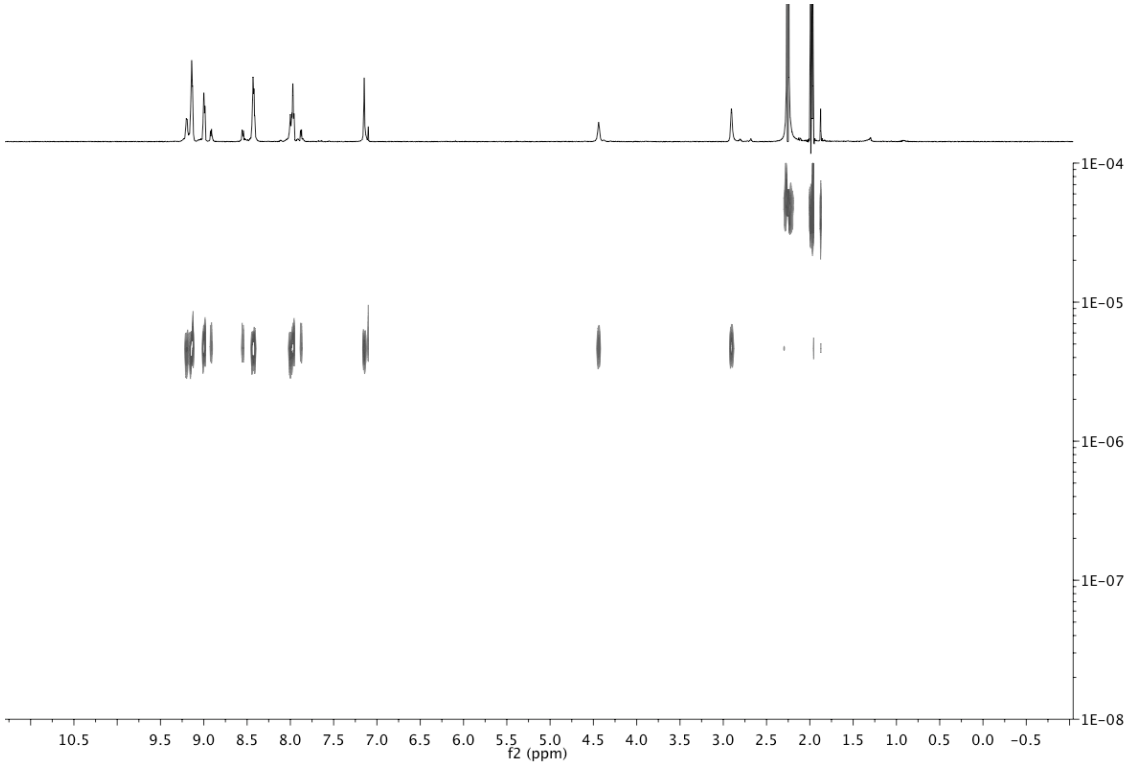

Figure S16: DOSY (CD_3CN, 500 MHz) spectrum of **5a**·$2BF_4$·4OTf·$8PF_6$

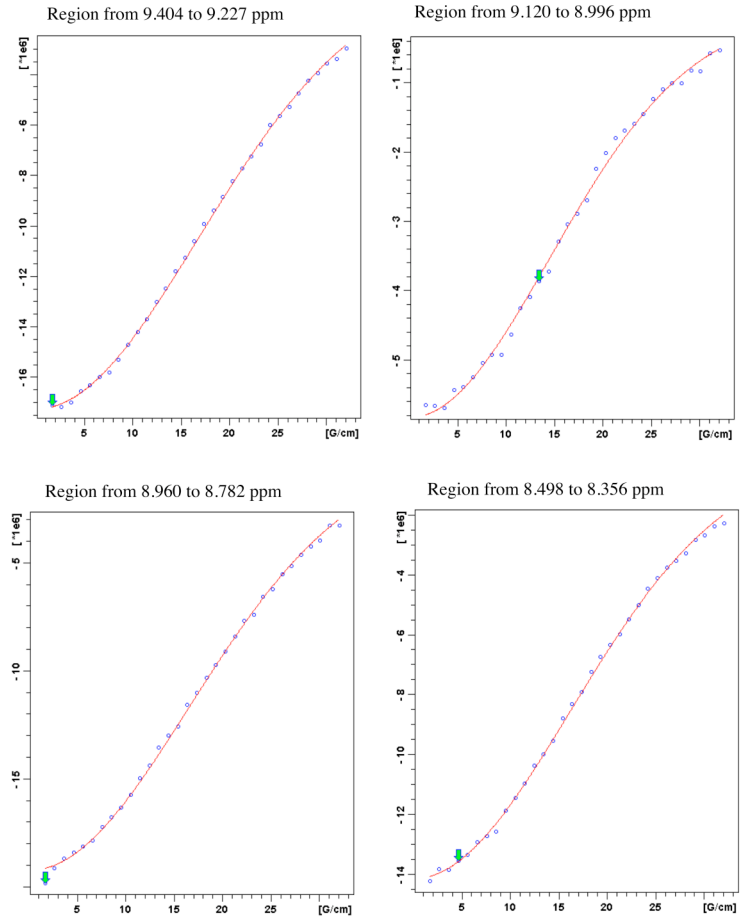

Figure S17: Fitting of I/I_o for some ^1H signals of compound **5a**·$2BF_4$·4OTf·$8PF_6$ to a simple one-component exponential.

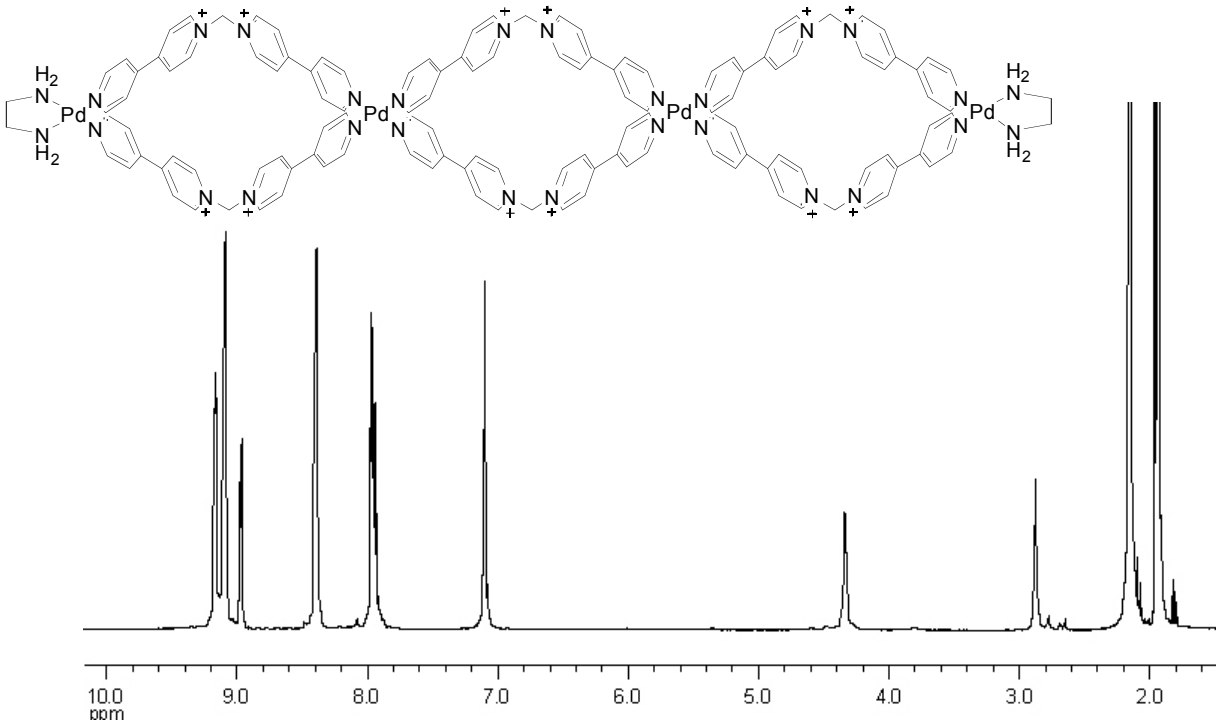

Figure S18: ^{1}H NMR (CD_3CN, 500 MHz) spectrum of **6a**·4BF_4·4OTf·12PF_6

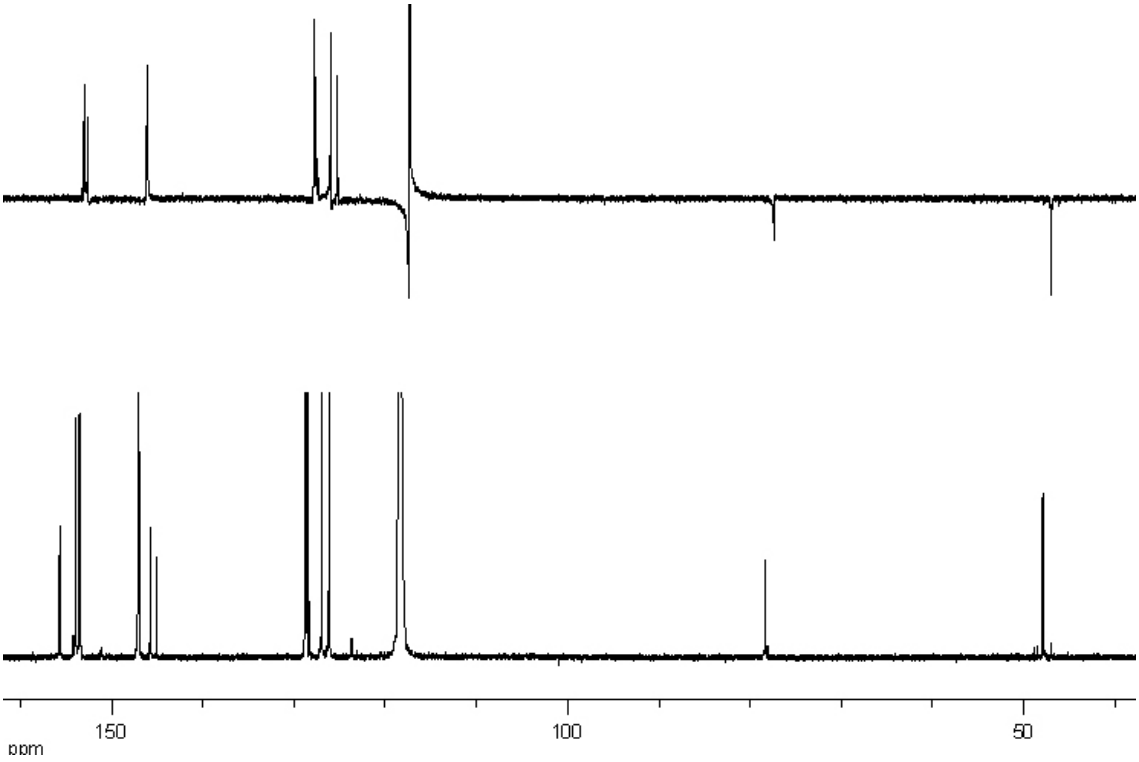

Figure S19: ^{13}C NMR (CD_3CN, 125 MHz) spectrum of **6a**·4BF_4·4OTf·12PF_6

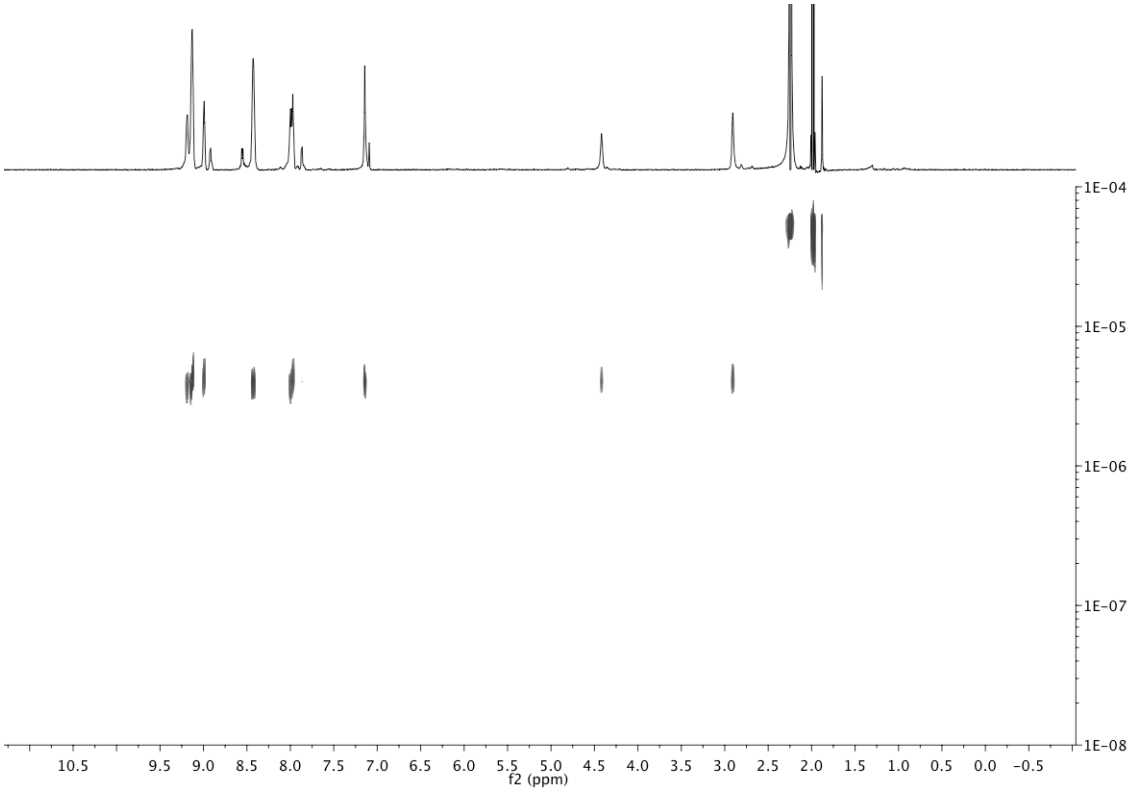

Figure S20: DOSY (CD_3CN, 500 MHz) spectrum of **6a**·$4BF_4$·4OTf·$12PF_6$

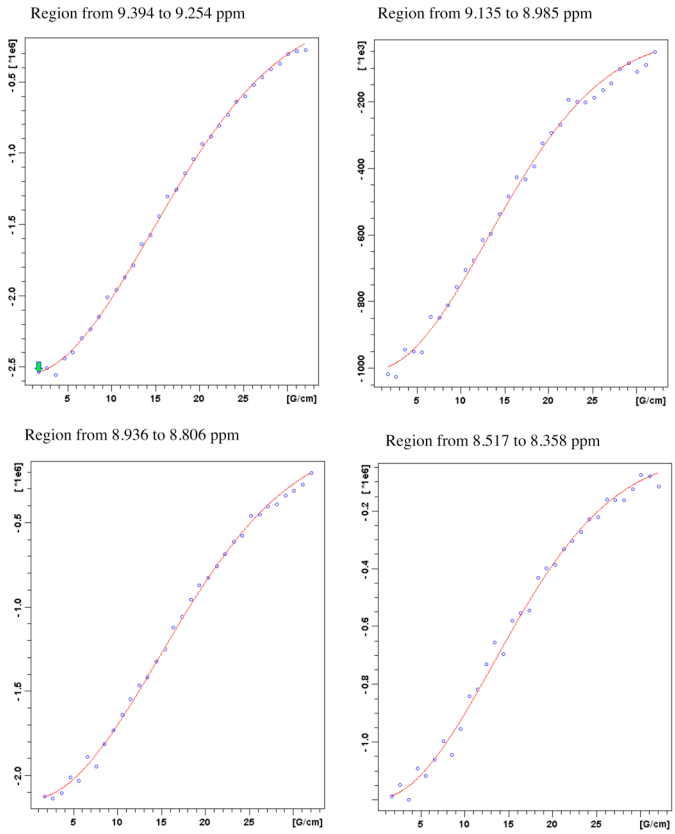

Figure S21: Fitting of I/I_o for some ^1H signals of compound **6a**·$4BF_4$·4OTf·$12PF_6$ to a simple one-component exponential.

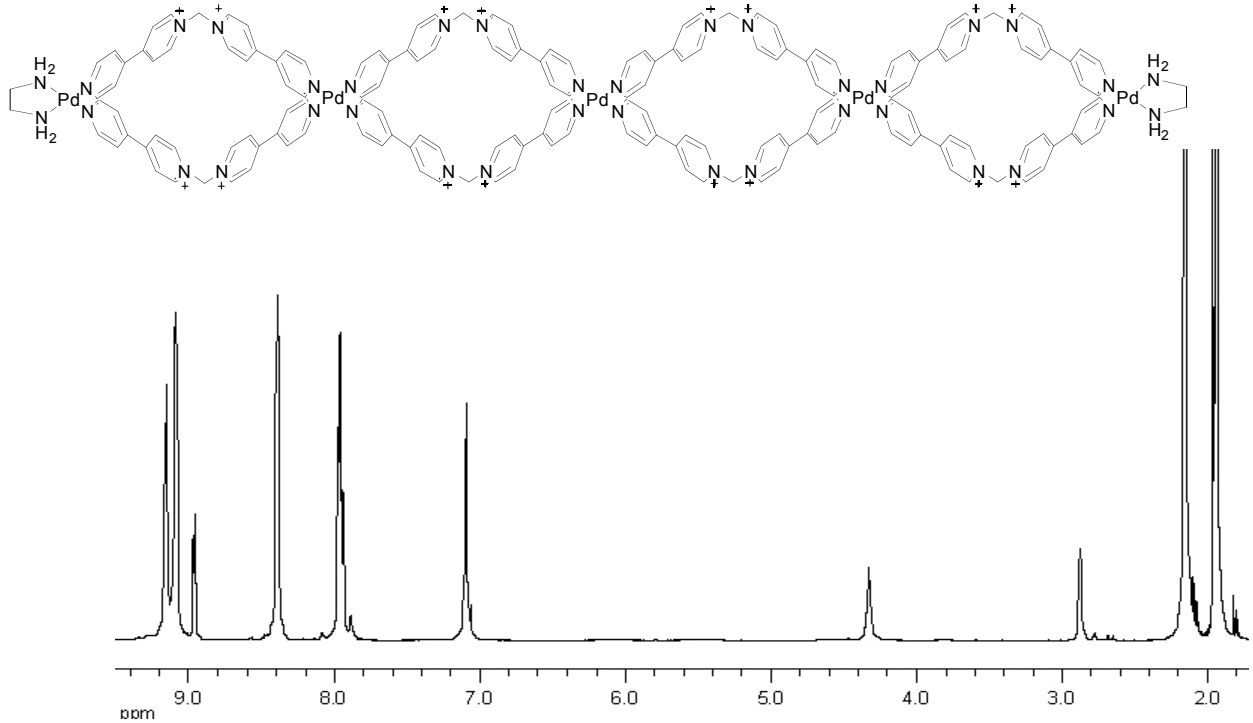

Figure S22: ^{1}H NMR (CD_3CN, 500 MHz) spectrum of **7a**·6BF_4·4OTf·16PF_6

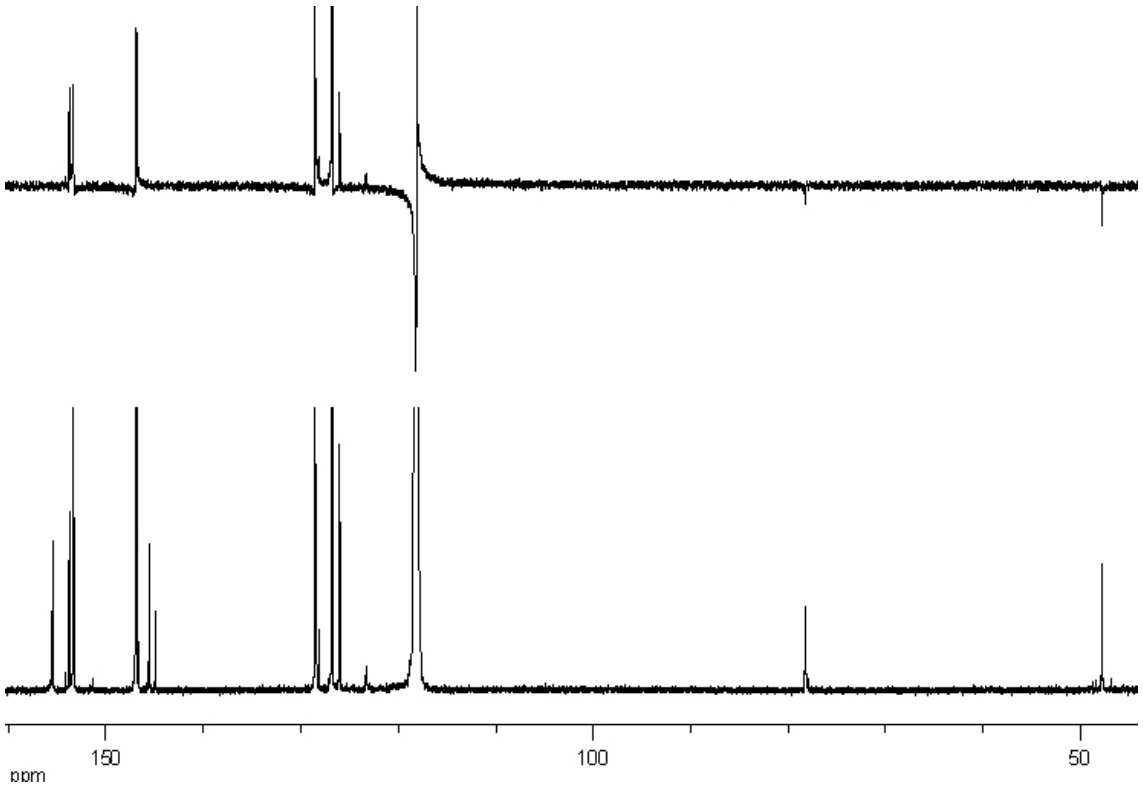

Figure S23: ^{13}C NMR (CD_3CN, 125 MHz) spectrum of **7a**·6BF_4·4OTf·16PF_6

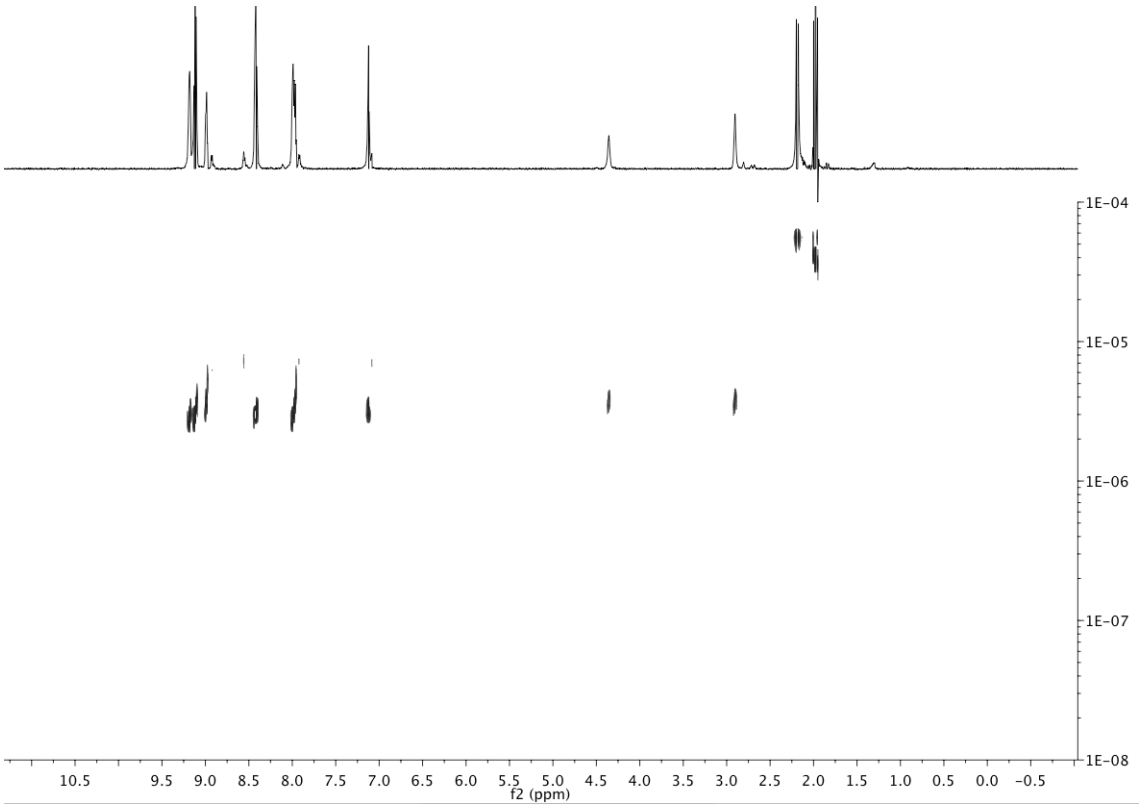

Figure S24: DOSY (CD_3CN, 500 MHz) spectrum of **7a**·6BF_4·4OTf·16PF_6

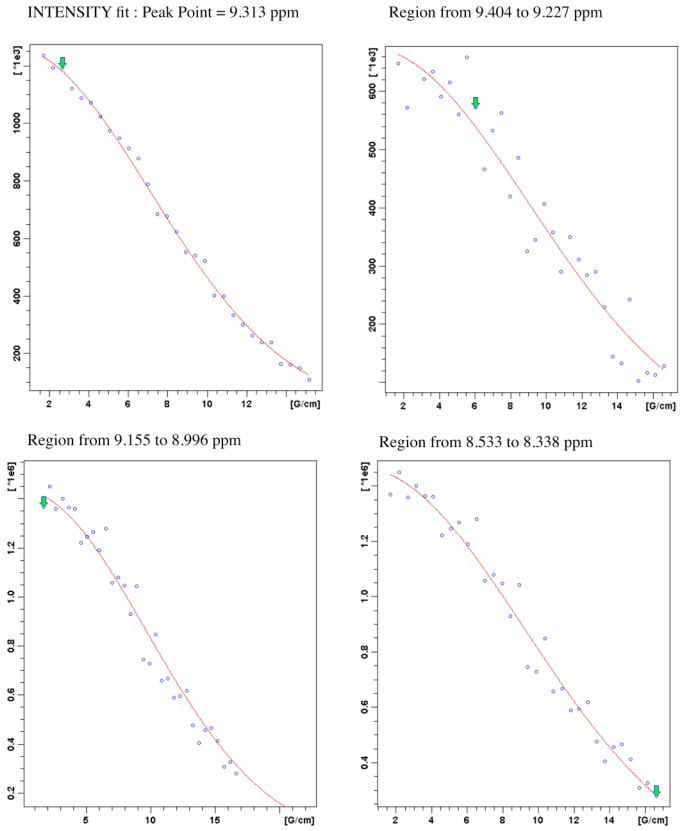

Figure S25: Fitting of I/I_o for some ^1H signals of compound **7a**·6BF_4·4OTf·16PF_6 to a simple one-component exponential.

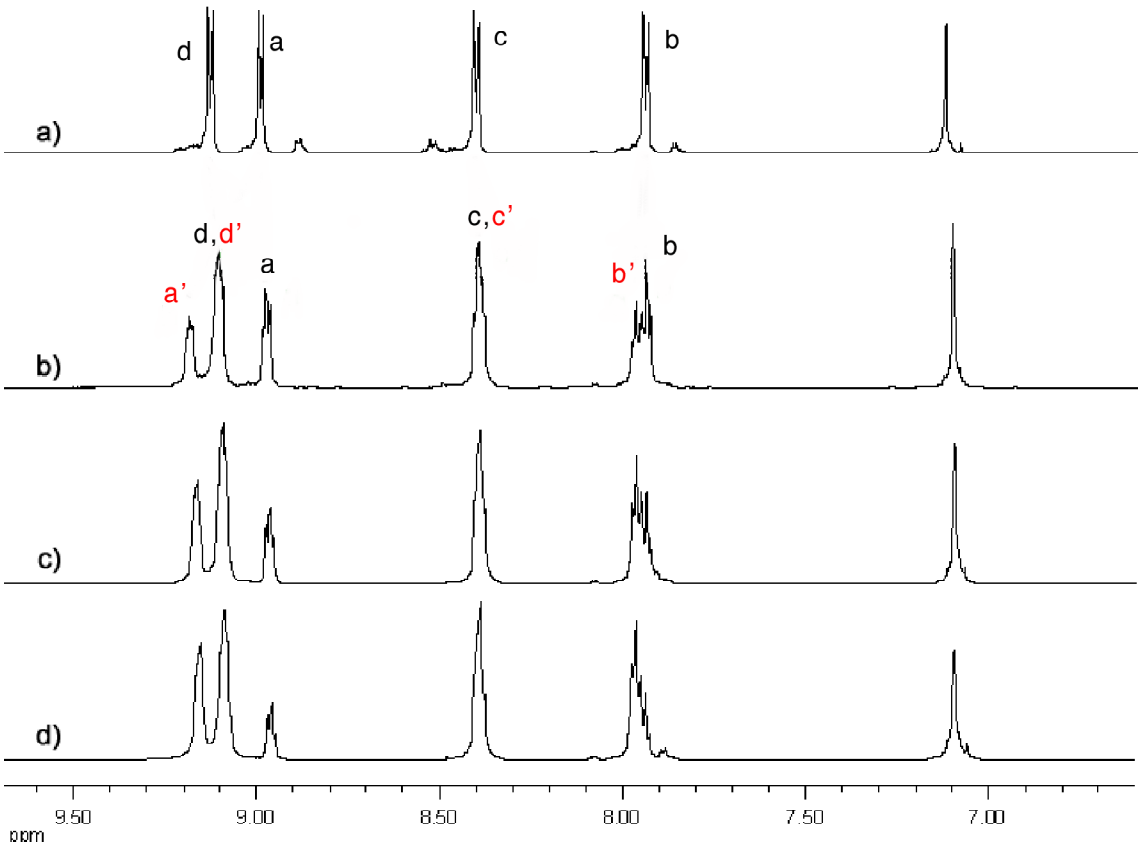

Figure S26: Partial ^{1}H NMR (CD_3CN, 500 MHz) spectra of: a) **4a**·4OTf·4PF_6, b) **5a**·2BF_4·4OTf·8PF_6, c) **6a**·4BF_4·4OTf·12PF_6, d) **7a**·6BF_4·4OTf·16PF_6

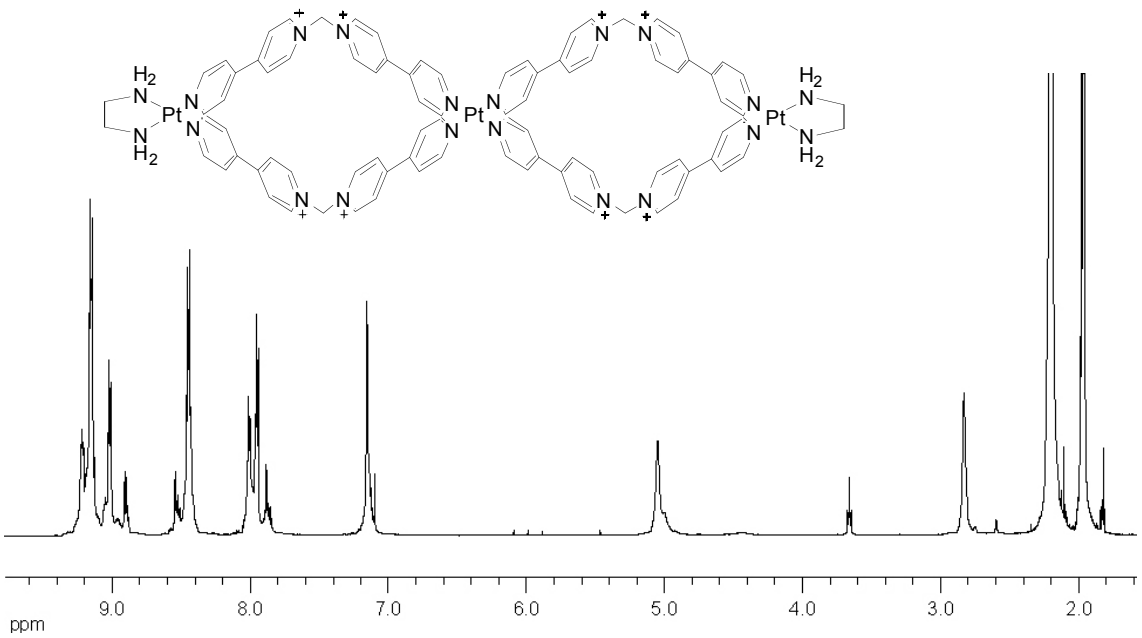

Figure S27: ^{1}H NMR (CD_3CN, 500 MHz) spectrum of **5b**·14PF_6

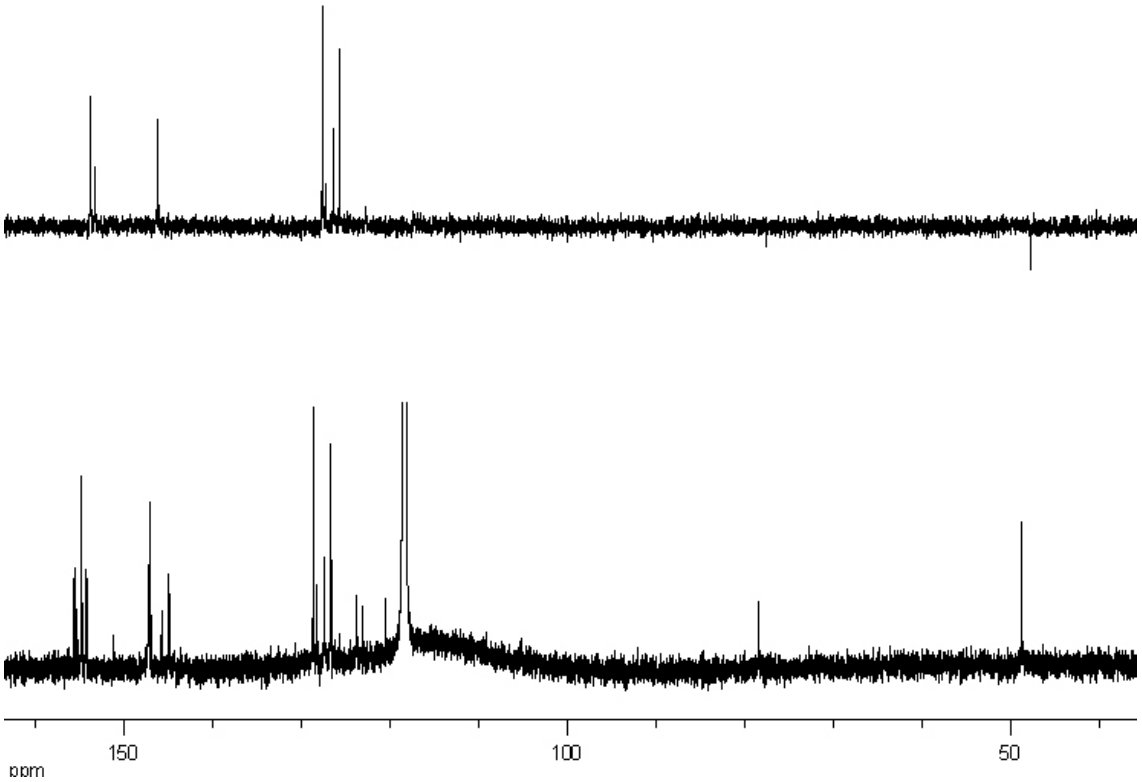

Figure S28: ^{13}C NMR (CD_3CN, 125 MHz) spectrum of **5b**·14PF_6

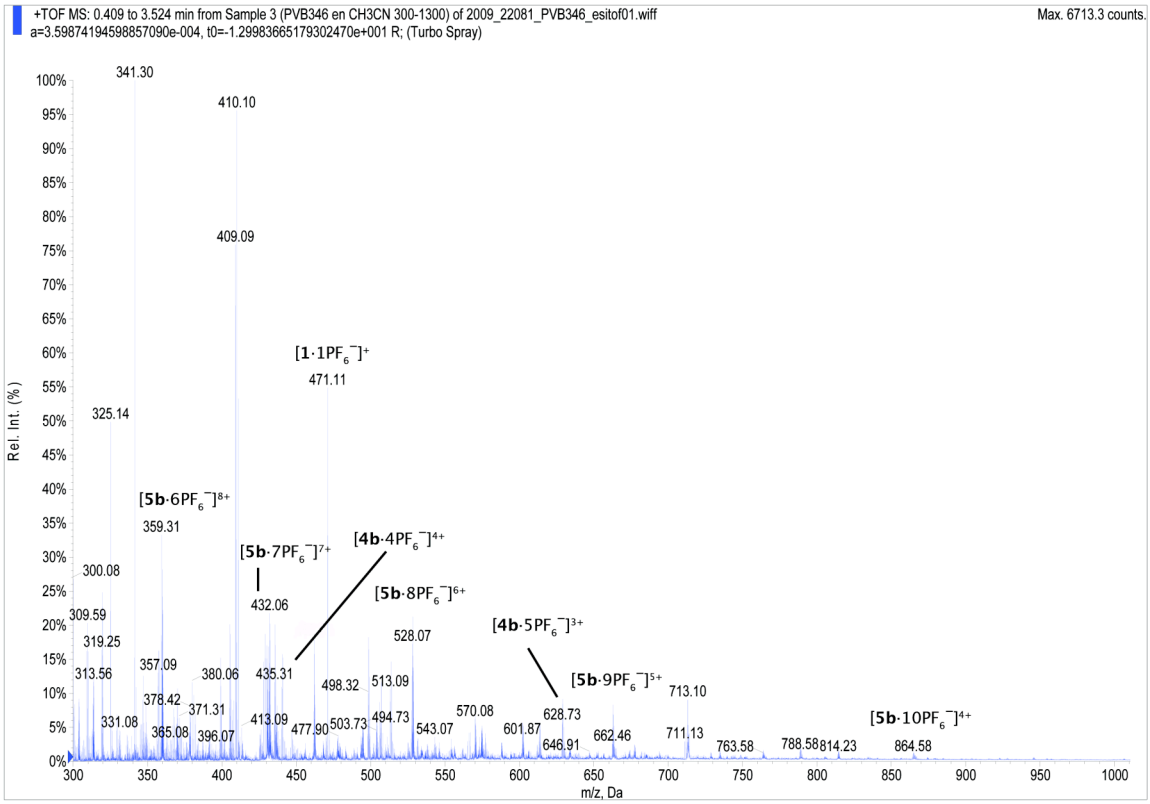

2009_22081_PVB346_esitof02

Figure S29: ESI-MS of **5b**·14PF_6.

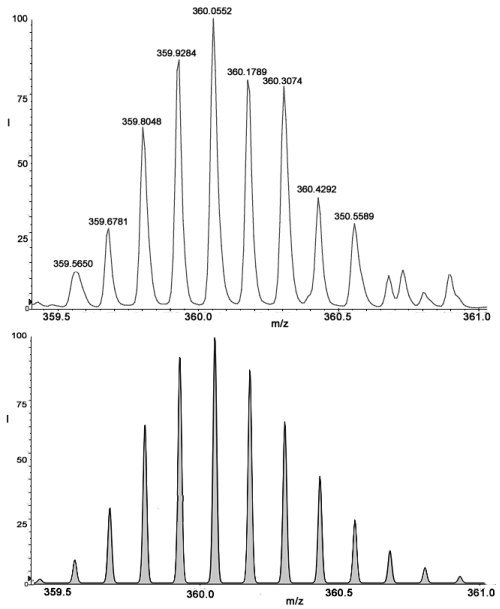

Figure S30: Observed (top) and theoretical (bottom) isotopic distribution for the fragment [**5b**·6PF_6]$^{+8}$.

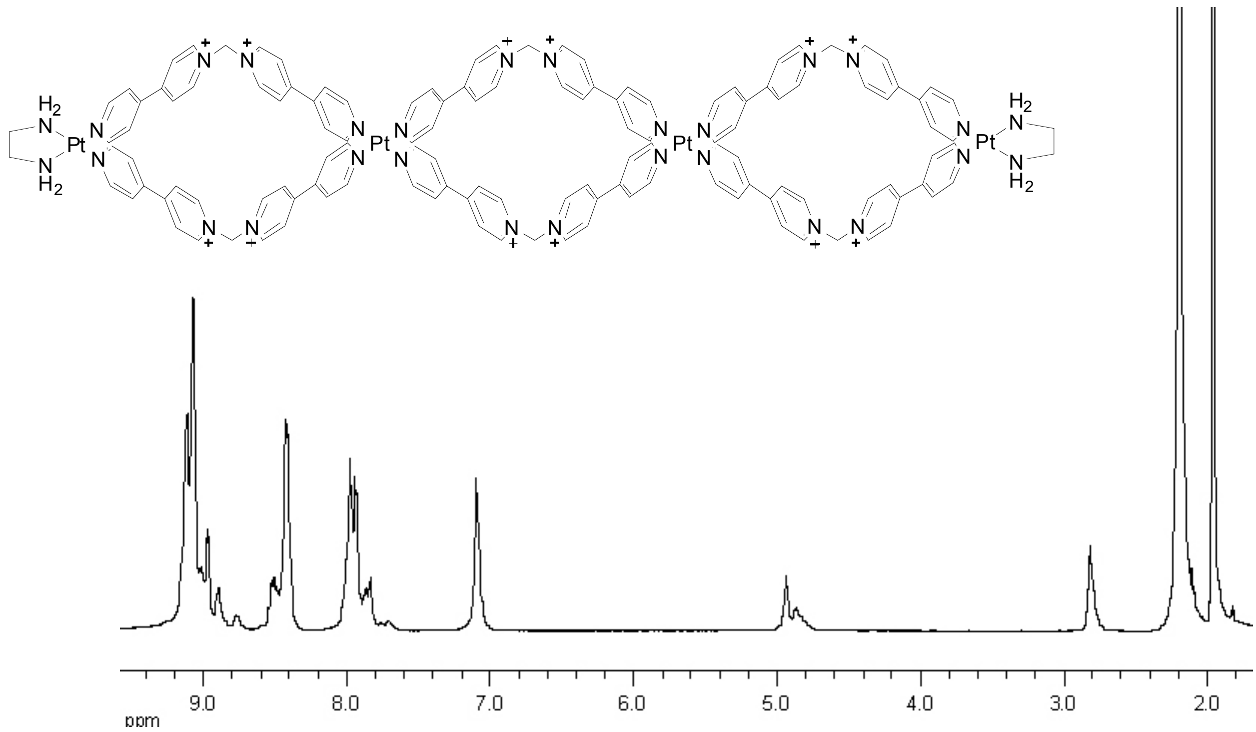

Figura S31: ^{1}H NMR (CD_3CN, 500 MHz) spectrum of **6b**·$20PF_6$

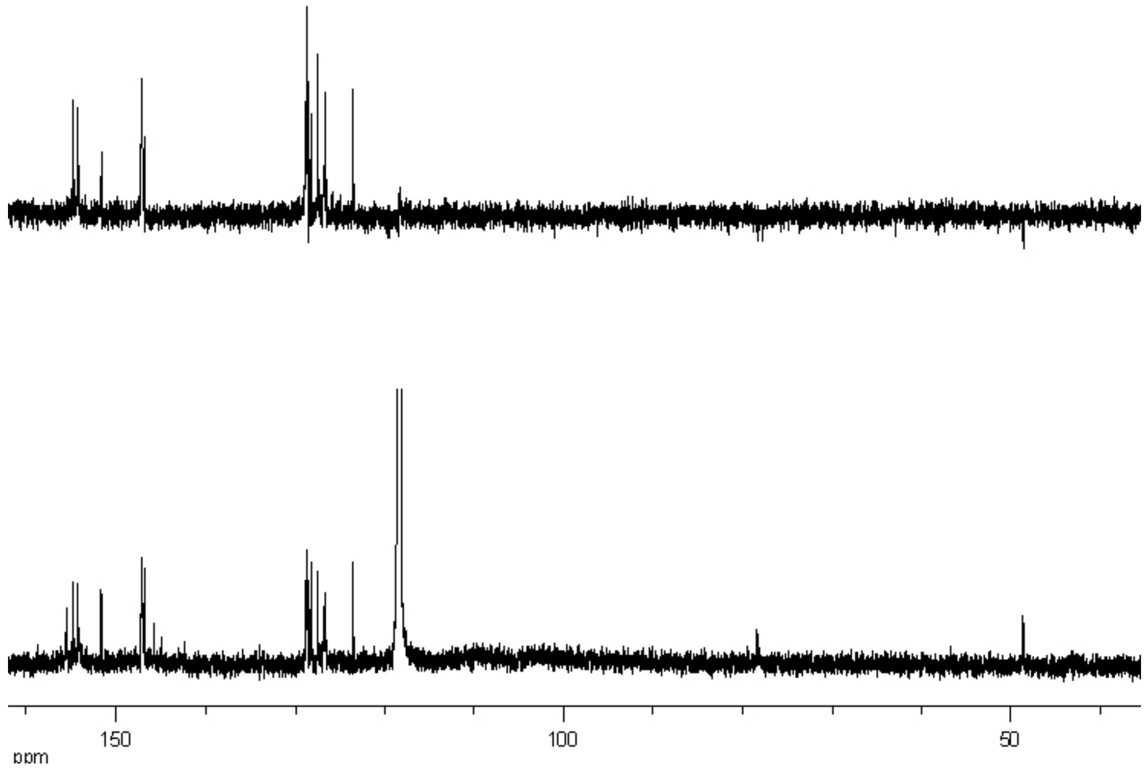

Figure S32: ^{13}C NMR (CD_3CN, 125 MHz) spectrum of **6b**·$20PF_6$

Sample Name	EM6299	**Position**	P1-A8	**Instrument Name**	Instrument 1	**User Name**	
Inj Vol	2	**InjPosition**		**SampleType**	Sample	**IRM Calibration Status**	Success
Data Filename	MSD5293.d	**ACQ Method**	ESIpos.m	**Comment**	MD PUB 347 (M. Ferrer)	**Acquired Time**	11/26/2009 11:00:29 AM

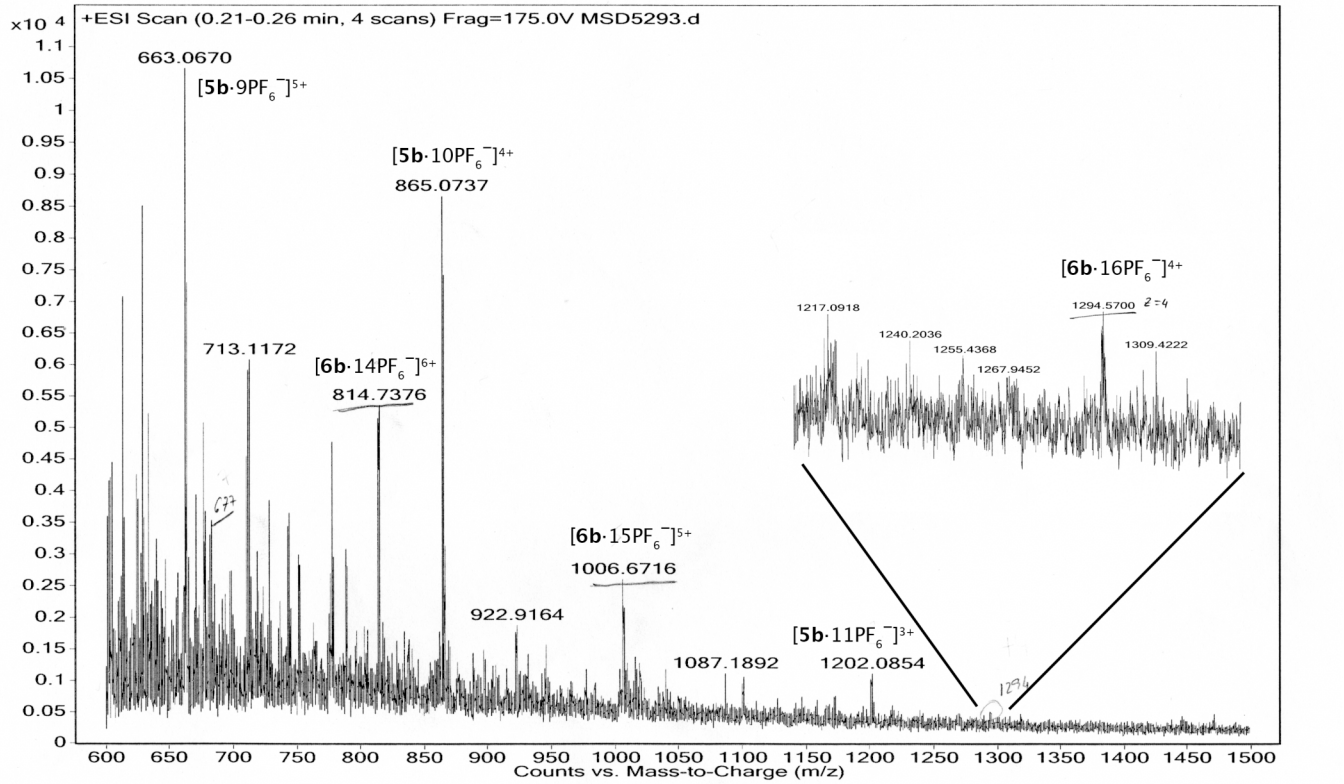

Figure 33: ESI-MS of **6b**·20PF_6.

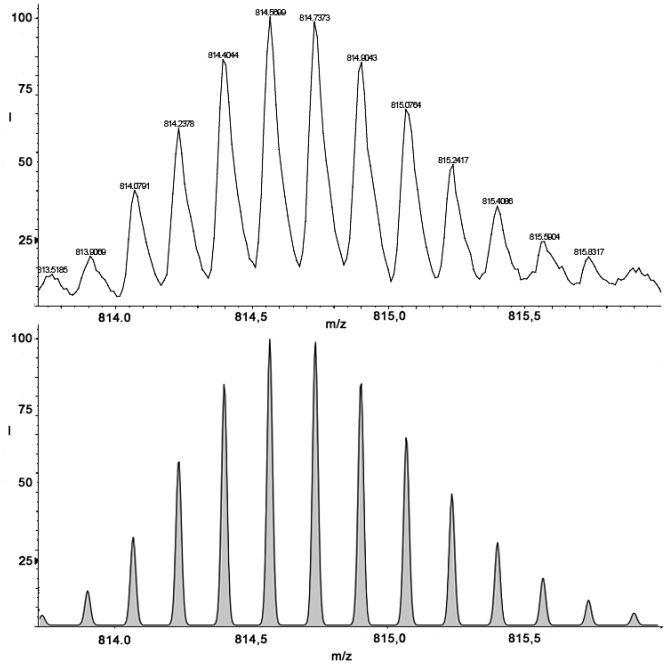

Figure 34: Observed (top) and theoretical (bottom) isotopic distribution for the fragment [**6b**·14PF_6]$^{+6}$.

Dynamic formation of dimer, trimer, and tetramer in D_2O.

Three stock solutions were prepared: solution A: 20 mM of **1**·$2NO_3$, solution B: 20 mM of **2a**, solution C: 10 mM of **3a**·$2BF_4$ 0.3 mL of solution A were mixed with 0.3 mM of solution B. To this solution were added 0.3 mL of A and 0.30 mL of C. This addition was repeated twice. To the resulting solution of tetramer 0.15 mL of solution A and 0.15 mL of solution B were added, and finally 0.45 mL of A and 0.45 mL of B were added. Upon each addition an aliquot was extracted and a ^{1}H NMR spectrum was recorded, which were identical to those obtained and reported above.

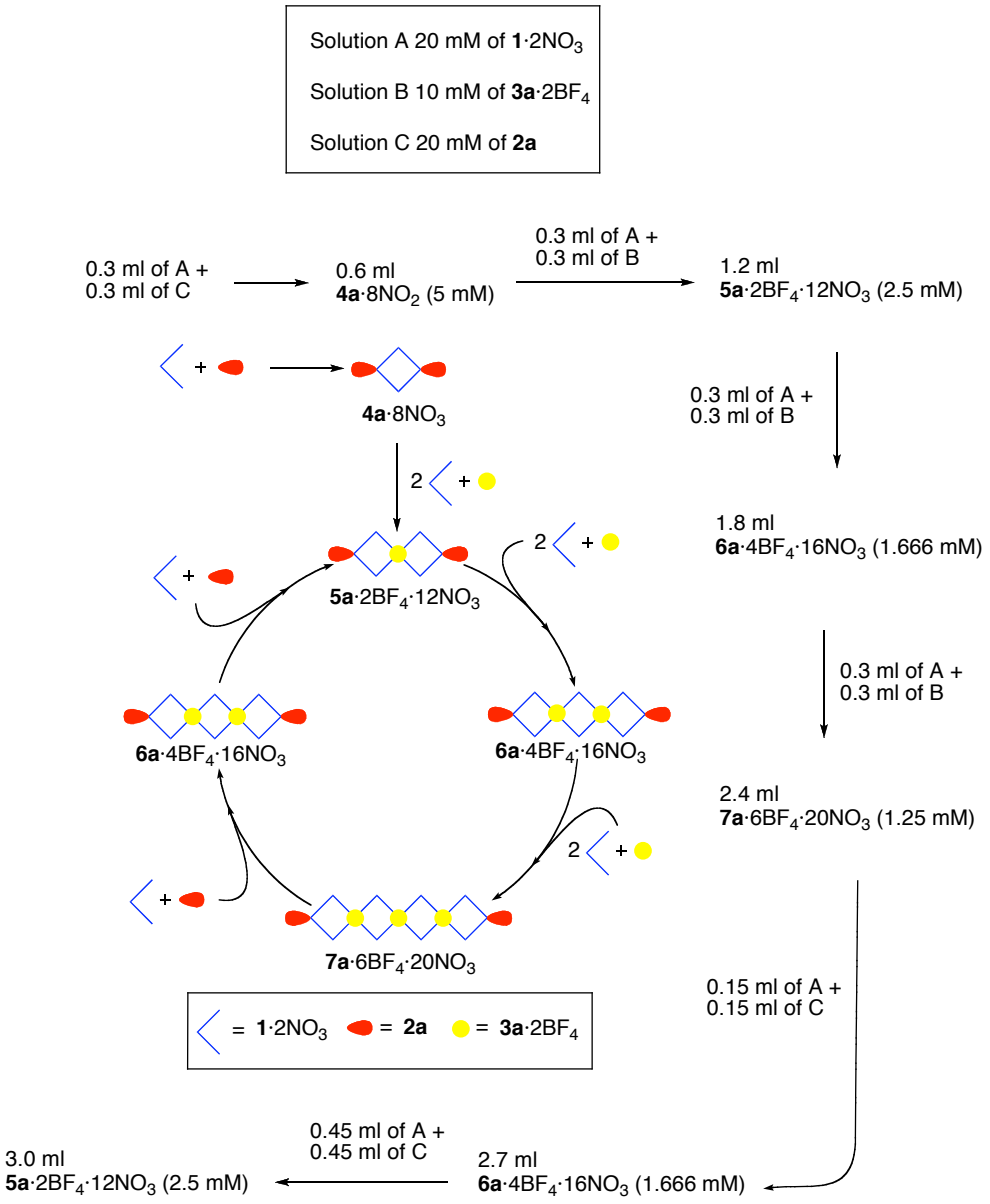

Determination of diffusion coefficients from theoretical models

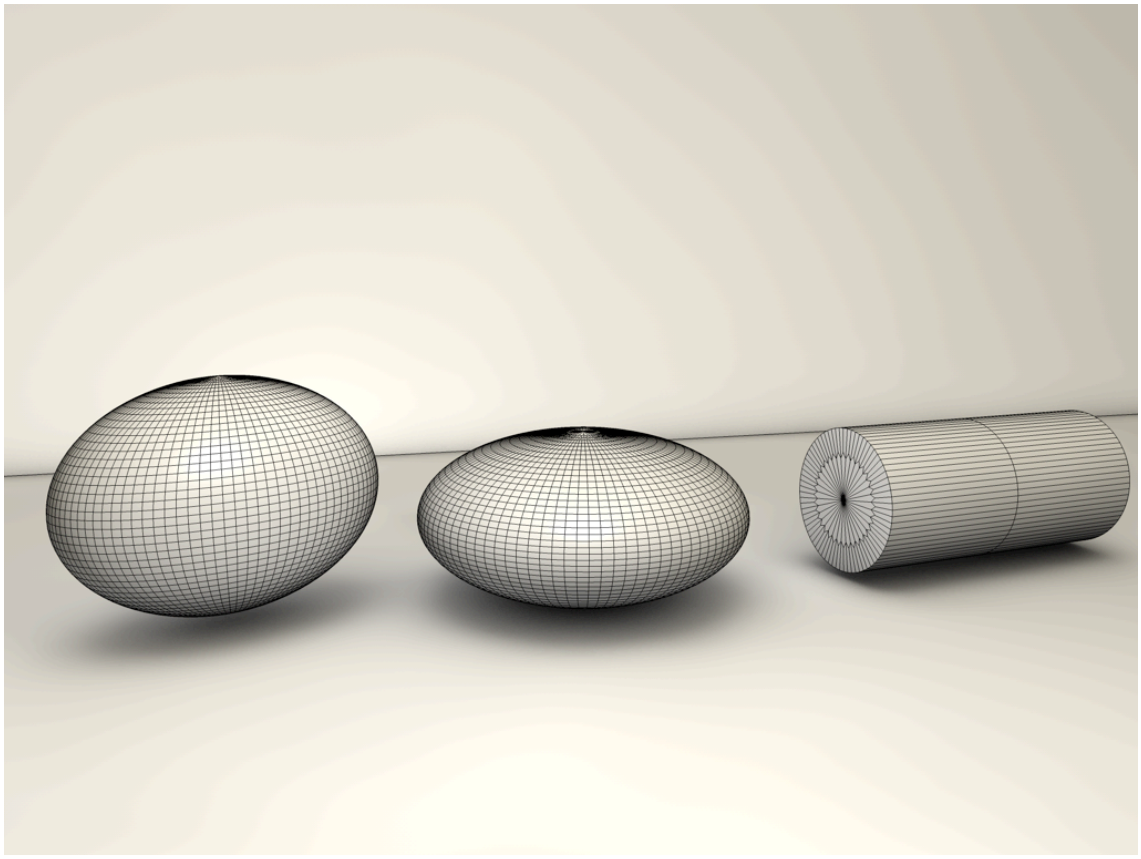

Diffusion coefficients were calculated according to three models: prolate ellipsoid (left), oblate ellipsoid (center) and cylindrical (right).

$$D = \frac{k_B T}{6\pi\mu R f}$$

k_B, Boltzmann constant, T, temperature, R, hydrodynamic radius, f correction factor of each model, and μ viscosity (D_2O, 1.232×10^{-3} Pa s at 298 K)[5]

Model: Prolate ellipsoid

$$R = \sqrt[3]{ab^2}$$

$$f = \frac{P^{-1/3}\sqrt{P^2-1}}{\ln\left(P+\sqrt{P^2-1}\right)}$$

Where P = a/b

[5] (a) Wheate, N. J.; Anil Kumar, P. G.; Torres, A. M.; Aldrich-Wright, J. R.; Price, W. S. *J. Phys. Chem. B* **2008,** *112,* 2311. (b) G. Jones, H. J. Fornwalt, *J. Chem. Phys.* **1936,** *4*, 30.

	a	b	R	P	f	*D*	-log *D*
4a	1.1086E-09	6.903E-10	8.08382E-10	1.60596842	1.02029443	2.1481E-10	**9.66795423**
5a	2.0397E-09	6.26E-10	9.27944E-10	3.2587474	1.13075773	1.6885E-10	**9.77250326**
6a	2.9994E-09	6.088E-10	1.03592E-09	4.92674113	1.24491217	1.3738E-10	**9.86207845**
7a	3.9769E-09	6.0075E-10	1.128E-09	6.61980857	1.352153	1.1616E-10	**9.9349466**

Model: Oblate ellipsoid

$$R = \sqrt[3]{a^2 b}$$

$$f = \frac{P^{-2/3}\sqrt{P^2 - 1}}{\arctan\left(\sqrt{P^2 - 1}\right)}$$

P = a/b

	a	b	R	P	f	D	-log D
4a	1.11E-09	1.97E-10	6.23738E-10	5.61458597	1.256656216	2.26032E-10	**9.64583062**
5a	2.04E-09	1.97E-10	9.36532E-10	10.329957	1.470748218	1.28625E-10	**9.89067299**
6a	3.00E-09	1.97E-10	1.21109E-09	15.1906812	1.642112597	8.90861E-11	**10.0501901**
7a	3.98E-09	1.97E-10	1.46166E-09	20.1410484	1.78645823	6.785E-11	**10.1684499**

Model: Cylinder

$$R = \sqrt[3]{\frac{3ab^2}{2}}$$

$$f = \frac{(2/3)^{1/3} P^{2/3}}{\ln(2P) - 0.3}$$

	a	b	R	P	f	*D*	-log *D*
4a	1.1086E-09	6.903E-10	9.2537E-10	1.60596842	1.38198991	1.3854E-10	**9.85843067**
5a	2.0397E-09	6.26E-10	1.0622E-09	3.2587474	1.21954207	1.3676E-10	**9.86402757**
6a	2.9994E-09	6.088E-10	1.1858E-09	4.92674113	1.27242232	1.1742E-10	**9.9302681**
7a	3.9769E-09	6.0075E-10	1.2912E-09	6.61980857	1.34892142	1.0172E-10	**9.99260451**

Table S1. Diffusion coefficients and dimensions of metallocycles

Compound	-log*D* (m^2s^{-1})	Calculated dimensions A × B (nm)[a]	Calculated -log*D* (m^2s^{-1})
4b	9.64	2.22 × 1.38[c]	9.64[c]
5a	9.8	4.08 × 1.25	9.86[d]
6a	9.9	6.00 × 1.22	9.93[d]
7a	10.0	7.95 × 1.20	9.99[d]

[a] A is the distance between the diagonally opposite methylene carbons of the ethyelenediamine ligands in the modeled structures. B is the larger distance between opposite methylene groups of the bipyridinium ligands. [b] Distances measured in the Pd analog. [c] Value fitted according to oblate ellipsoidal model. [d] Value fitted according to cylindrical model.

Computational Methods

Full geometry optimizations of the **4a-7a** systems were performed at the HF level by using the Gaussian 03 program package (Revision C.01)[1]. In these calculations we used the standard 3-21G basis set for C, H and N atoms, while for Pd the LanL2DZ valence and effective core potential functions were used.[2] The stationary points found on the potential energy surfaces as a result of the geometry optimizations on the **4a** and **5a** systems have been tested to represent energy minima rather than saddle points via frequency analysis. Due to the consierable effort involved in the calculation of second derivatives, the optimized geometries of **6a** and **7a** were not characterized through frequency calculations.

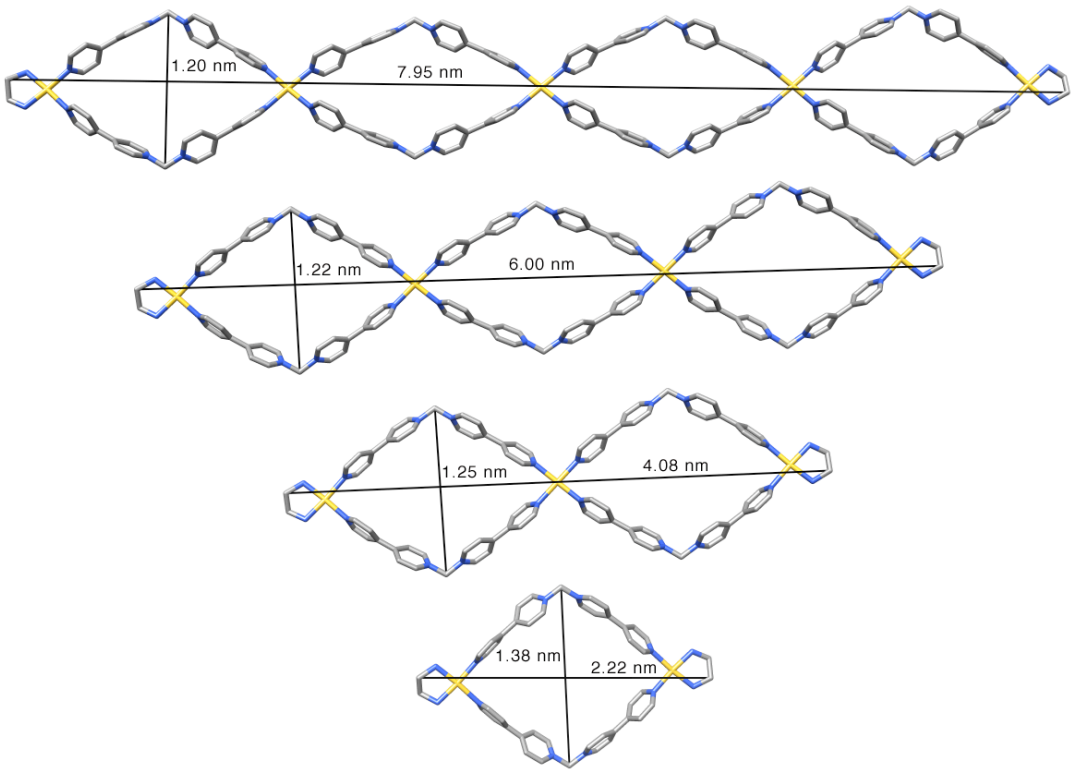

Figure 35: Calculated structures of **4a-7a**.

([1]) M. J. Frisch, G. W. Trucks, H. B. Schlegel, G. E. Scuseria, M. A. Robb, J. R. Cheeseman, J. A., Jr. Montgomery, T. Vreven, K. N. Kudin, J. C. Burant, J. M. Millam, S. S. Iyengar, J. Tomasi, V. Barone, B. Mennucci, M. Cossi, G. Scalmani, N. Rega, G. A. Petersson, H. Nakatsuji, M. Hada, M. Ehara, K. Toyota, R. Fukuda, J. Hasegawa, M. Ishida, T. Nakajima, Y. Honda, O. Kitao, H. Nakai, M. Klene, X. Li, J. E. Knox, H. P. Hratchian, J. B. Cross, C. Adamo, J. Jaramillo, R. Gomperts, R. E. Stratmann, O. Yazyev, A.

J. Austin, R. Cammi, C. Pomelli, J. W. Ochterski, P. Y. Ayala, K. Morokuma, G. A. Voth, P. Salvador, J. J. Dannenberg, V. G. Zakrzewski, S. Dapprich, A. D. Daniels, M. C. Strain, O. Farkas, D. K. Malick, A. D. Rabuck, K. Raghavachari, J. B. Foresman, J. V. Ortiz, Q. Cui, A. G. Baboul, S. Clifford, J. Cioslowski, B. B. Stefanov, G. Liu, A. Liashenko, P. Piskorz, I. Komaromi, R. L. Martin, D. J. Fox, T. Keith, M. A. Al-Laham, C. Y. Peng, A. Nanayakkara, M. Challacombe, P. M. W. Gill, B. Johnson, W. Chen, M. W. Wong, C. Gonzalez, J. A. Pople, Gaussian, Inc., Wallingford CT, 2004.

([2]) P. J. Hay, W. R. Wadt, *J. Chem. Phys*. 1985, **82**, 270-283..